Received 30 November 2023; revised 17 December 2023; accepted 19 December 2023. Date of publication 26 December 2023; date of current version 12 January 2024.

Digital Object Identifier 10.1109/OJCOMS.2023.3347388

Analysis of Multi-User-Based UAV System With Outdated CSI

PARVEZ SHAIK [1] (Member, IEEE), CIHAT KEÇECI [2], KAMAL K. GARG [3], MUHAMMAD ISMAIL [4] (Senior Member, IEEE), AND ERCHIN SERPEDIN [2] (Fellow, IEEE)

[1] Electrical and Computer Engineering Program, Texas A&M University at Qatar, Doha, Qatar

[2] Department of Electrical and Computer Engineering, Texas A&M University at College Station, College Station, TX 77843, USA

[3] School of Technology, Pandit Deendayal Energy University, Gandhinagar 382009, India

[4] Department of Computer Science, Tennessee Tech University, Cookeville, TN 38505, USA

CORRESPONDING AUTHOR: P. SHAIK (e-mail: parvez.shaik@qatar.tamu.edu)

This work was supported by the Qatar National Research Fund (a member of Qatar Foundation) NPRP Grant under Grant NPRP13S-0127-200182. Open Access funding provided by the Qatar National Library.

ABSTRACT In this paper, we investigate the performance of multiple-input and multiple-output (MIMO) unmanned air vehicle (UAV) based multi-user communication systems over generalized Nakagami-m fading channels subject to channel feedback delays. The impact of decode-and-forward (DF) based relaying and outdated channel state information is assessed at the receiver nodes. To reduce the complexity and retain the MIMO gains, the transmit antenna selection (TAS) strategy is used to select the best antenna at the source and UAV nodes. A generic framework in the form of closed-form analytical expressions for outage probability (OP), asymptotic OP, and the average symbol error rate of higher-order quadrature amplitude modulation (QAM) schemes such as hexagonal QAM, rectangular QAM, and cross QAM are derived. In addition, energy efficiency analysis is also performed for the considered system model. In this framework, altitude and location-dependent path loss modeling are considered for the air-to-ground links. Optimization of UAV location and altitude is performed through a limited-memory Broyden-Fletcher-Goldfarb-Shanno (LBFGS) algorithm to attain minimum OP (MOP). Results illustrate optimal performance dependent on the channel correlation parameters, antenna elements, and fading conditions. Monte-Carlo simulations are performed to validate the derived analytical results and compared with the existing works.

INDEX TERMS UAV, MIMO, TAS, DF, LBFGS optimization, HQAM, RQAM, XQAM, Nakagami-m, outdated CSI.

I. INTRODUCTION

Unmanned aerial vehicles (UAVs) are anticipated to play a significant role in future wireless communications in catering highly reliable services to civilian, commercial, military, and critical emergency applications where the terrestrial communications cease to operate [1]. UAVs have revolutionized wireless communications with salient features such as flexible rapid networking and deployment abilities, controlled mobility with design degrees of freedom, robust connectivity with LOS with enhanced coverage area, and spectrum efficiency [2]. ITU has authorized the use of a portion of the L-band for UAV applications. Large-scale UAV long-term evolution eNodeBs were proposed as potential replacements for terrestrial eNodeBs [3], [4]. Industry and academia have advanced to the next level of research and development to assess the potential of UAVs as flying BSs and flying relays via field-trialed prototypes [5], [6]. With the evident benefits and multitude of opportunities, UAV-aided wireless communications are expected to be an integral part of the future 6G telecommunications systems.

A. RELATED WORKS

UAVs are classified as LAPs and HAPs based on the altitude and range of operation. LAPs are used to assist cellular communications and provide short-range LOS links with significant coverage area [7]. UAVs in cellular communications are employed in a cooperative fashion to regulate the diversity in a virtual MIMO scenario by sharing the resources between the source and the destination nodes to enhance the area of coverage and establish a reliable communication link [8]. Zhan et al. [9] studied UAV relaying-based terrestrial communications over Rayleigh fading channels and optimized the performance of ground-to-relay links by controlling UAV heading angle. The optimization of the altitude of a UAV to maximize the area of coverage for the radio signals was conducted in [10]. In [11], mobile UAVs were explored to maximize the throughput by optimizing the source/relay transmit power along with the trajectory. An air-to-ground UAV-based cooperative system was investigated in [12] and analytical expressions for the optimal height to achieve MOP were also presented. Chen et al. [13] reported minimum OP by optimal placement of UAV and analyzed the BER of BPSK modulated signal over Nakagami-m fading channels. However, these works are confined to SISO systems and perfect CSI conditions.

From the perspective of cognitive networks, [14] analyzed the achievable rates of an uplink cognitive radio for a UAV relay-assisted MIMO system over Rician fading channels for an uplink scenario with respect to interference and power constraints. In addition, it derived the optimal power allocation to maximize the achievable rates and examined the impact of UAV altitude over achievable rates for the primary and secondary users. A comparative study of multi-hop and multiple dual-hop UAV relays is presented in [15]. This study assesses the BER of BPSK along with the optimum location and altitude of the UAV. The study [16] investigated the AF based MIMO UAV relaying swarm system and derived the upper bound of capacity for the optimal position of UAVs within the swarm specifically for LoS channels. Hosseinalipour et al. [17] examined the impact of RF interference on the performance of UAV relays, and presented the optimal position of UAV to maximize the signal-to-interference-ratio (SIR) of the system by considering dual-hop and multi-hop communication schemes.

On the other hand, in cellular communications, digital modulation schemes especially energy-efficient QAM schemes play a significant role in spectral and power-efficient transmissions. The family of QAM schemes includes square QAM, rectangular QAM, cross QAM, and hexagonal QAM [18]. Significant studies were carried out recently over the ASER of higher-order QAM schemes in RF communications, OWC (especially UVC and FSO), and in mixed RF/OWC [19], [20], [21], [22], [23], [24], [25]. Studies [13], [15] confined the BER analysis of the SISO UAV relaying system for the BPSK modulation. Reference [26] considered a satellite-based system with SISO source and UAV relay with multi-users and investigated ASER of HQAM, RQAM, and XQAM.

B. MOTIVATION

The majority of the works presented have provided deep insights into designing and modeling UAV relay-based communications. However, their analysis is confined to SISO and multi-UAV relay-based systems and very few limited MIMO-based system models with perfect CSI conditions for simpler channels. To handle emergencies (such as natural disasters) integrated non-terrestrial-terrestrial networks are widely employed to enable the deployment of terrestrial infrastructures, which in general are economically infeasible and challenging. Thus, UAVs are employed to set up reliable links with guaranteed QoS indicators. MIMO antenna systems not only improve the spectral efficiency but also reliability and coverage area [27]. To leverage the agility of UAVs along with the MIMO antennas, it is very timely and interesting to investigate the performance of MIMO systems. However, considering perfect channel conditions under such scenarios is practically infeasible. Due to the dynamic nature of the time-varying wireless channels (induced by the motion of the transmitter, receiver, or both), perfect CSI at the transmitter is unavailable. Moreover, antenna selection in MIMO systems gets affected by the outdated CSI which degrades the system performance. Thus, feedback delays and their impact on the system performance are considered. To the best of the authors' knowledge, analysis of MIMO UAV decode-and-forward (DF) relaying-based multi-user systems with outdated CSI over-generalized Nakagami-m fading channels is not available.

C. CONTRIBUTIONS

Hence, in this work, we consider UAV-assisted cooperative communication with multiple antennas at the transmitter, UAV relay, and multiple UEs with a single antenna. It is highly deterrent to use MIMO antenna systems due to the requirement of individual RF chains for each active antenna. Hence, to leverage MIMO antenna gains and to reduce hardware complexity, TAS is used. In addition, it is considered that the system operates at very high frequencies and the spacing between the antennas is sufficiently large to make them uncorrelated [28], [29]. Furthermore, the location and altitude of the UAV are optimized under detrimental channel conditions. The major contributions of this work are next listed.

- Performance of UAV-assisted cooperative communication with multiple antennas at the transmitter and DF-based UAV relay with single antenna multi-users is investigated by considering the feedback delays over the entire communication link. The CDF for the e2e SNR for the OP is derived by considering the TAS strategy.
- Asymptotic analysis is performed to determine the diversity order of the system. The obtained curves demonstrate the effect of outdated CSI on the diversity order of the system.

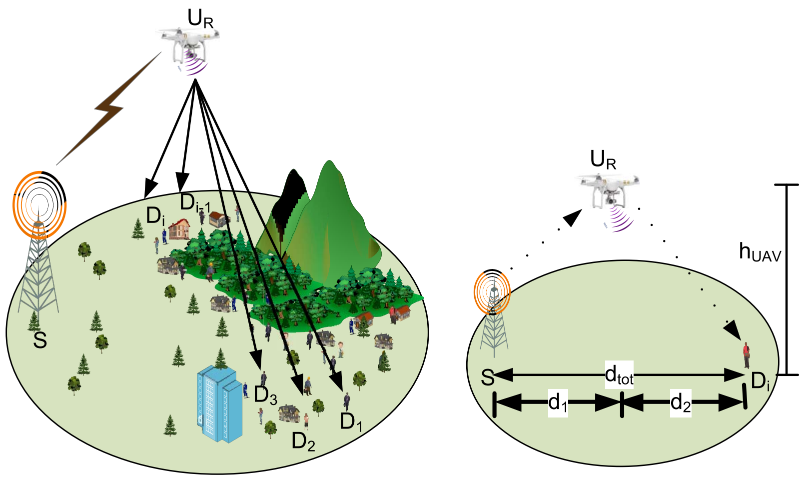

FIGURE 1. UAV based multi-user system model.

- Location of the UAV is optimized through the LBFGS algorithm to improve the system performance, capacity, and MOP.
- The UAV's altitude is also optimized to achieve the optimum performance of the system with MOP. The obtained results illustrate the dominance of UAV operational altitude over the MOP.
- ASER analysis of higher-order QAM modulation schemes is performed for HQAM, RQAM, and XQAM through closed-form expressions, and valuable insights are drawn.
- Energy efficiency analysis is carried to quantify the energy consumed in delivering data. Results illustrate the HQAM provides higher efficiency over other QAM schemes.
- System performance is analyzed for different numbers of antenna elements, channel fading conditions, and various channel correlation coefficients to draw deeper design insights. In addition, Monte-Carlo simulations are carried out to validate the correctness of the derived analytical expressions and to compare them with the existing works.

The rest of the paper is organized as follows. Section II presents the system model. Section III conducts the outage and asymptotic outage probability study. Optimization of the relay location and altitude are presented in Section IV. ASER analysis of higher-order QAM schemes is discussed in Section V. Section VI analyzes the numerical and simulation results. Section VII concludes the paper.

Notations: Matrices (column vectors) are denoted by bold uppercase (lowercase) letters; $(\cdot)^*$ and $(\cdot)^H$ stand for conjugate and complex conjugate transposition, respectively; $|\cdot|$ and $||\cdot||_F$ represent the magnitude and squared Frobenius norm, respectively. Nakagami-m distribution with fading severity $M_L = mN$ and variance Ω is denoted by $\mathrm{Nak}(\mathrm{M_L}, \Omega)$. The fading parameter is represented by m and number of receiver antennas by N; $\mathcal{CN}(0, \sigma^2\mathbf{I}_N)$ represents the complex Gaussian distribution with mean zero and covariance $\sigma^2\mathbf{I}_N$. $\mathbf{I}_N$ denotes the identity matrix of size $N \times N$. $U(0,1)$ stands for the uniform distribution with lower and upper bound 0 and 1, respectively. $\mathcal{J}_o(\cdot)$ identifies the zero-order Bessel function of first kind. ${}_1F_1(a,b,c)$ and ${}_2F_1(a,b,c,d)$ represent the confluent Hypergeometric function (HF) of first kind and Gauss HF, respectively. $Q(\cdot)$ stands for the Gaussian Q-function. $\mathbb{E}\{\cdot\}$ denotes the expected value.

II. SYSTEM MODEL

In this work, a dual-hop DF UAV-based system model with a MIMO BS with N_S antennas acting as a source (S) of information, MIMO DF-based UAV with N_{U_R} antennas acting as a relaying device ($\mathrm{U_R}$), and the K mobile users acting as destination node $\mathrm{D_i}$, $\mathrm{i} \rightarrow \{1, \ldots, L\}$ is considered as shown in FIGURE 1. Each UE is equipped with a single antenna due to size limitations. All UEs are assumed to be in close proximity and follow i.i.d. condition. We employ TAS to select a single transmit antenna that maximizes the received SNR at $\mathrm{U_R}$. Let $[\mathbf{h}_{\mathrm{AB}}^{(\mathrm{p})}]_{N_\mathrm{B}\times 1}$ be the channel vector corresponding to the $\mathrm{p^{th}}$ transmit antenna of the channel matrix $[\mathbf{H}_{\mathrm{AB}}]_{N_\mathrm{B}\times N_\mathrm{A}}$, where $\mathrm{A} \in \{\mathrm{S}, \mathrm{U_R}\}$, $\mathrm{B} \in \{\mathrm{U_R}, L\}$, and $\mathrm{A} \neq \mathrm{B}$. The UEs are scheduled opportunistically for multiuser diversity depending on the strongest link between the lth UAV antenna and the ith UE.

To characterize the best fading conditions, all the channel links are considered to be complex Nakagami-m frequency flat fading, $\mathrm{Nak}(\mathrm{M_L}, \hat{\Omega}_\mathbf{h})$ [30], [31]. Nakagami-m distribution provides greater flexibility in matching some empirical data than the Rayleigh, Lognormal, or Ricean distribution. It is a versatile statistical distribution that can accurately model Rayleigh and the one-sided Gaussian distribution. In addition, Ricean and Hoyt's distributions can be closely approximated. Moreover, for integer fading parameter values, Nakagami-m envelope is defined by the square root of the sum of squares of independent Rayleigh variates [32]. Further, it is assumed that all the links are affected by the

TABLE 1. List of acronyms and their descriptions.

2D	2 dimensional
6G	Sixth-generation
AWGN	Additive white Gaussian noise
AF	Amplify-and-forward
AG	Air-to-ground
ASER	Average symbol-error-rate
AWGN	Additive white Gaussian noise
BS	Base station
BER	Bit-error-rate
BPSK	Binary phase shift keying
CDF	Cumulative distribution function
CSI	channel state information
DF	Decode-and-forward
e2e	End-to-end
FSO	Free space optics
HQAM	Hexagonal QAM
HAPs	High-altitude platforms
i.i.d.	Independent and identically distributed
ITU	International Telecommunication Union
LAPs	Low-altitude platforms
LBFGS	Limited-memory Broyden-Fletcher-Goldfarb-Shanno
LOS	Line-of-sight
MIMO	Multiple-input and multiple-output
MMSE	Minimum mean square error
MOP	Minimum outage probability
OWC	Optical wireless communication
PDF	Probability density function
QAM	Quadrature amplitude modulation
QoS	Quality-of-service
RF	Radio frequency
RQAM	Rectangular QAM
SQAM	Square QAM
SER	Symbol-error-rate
SEP	Symbol-error-probability
SIR	Signal-to-interference-ratio
SNR	Signal-to-noise ratio
TAS	Transmit antenna selection
UAVs	Unmanned aerial vehicles
UVC	Ultraviolet communication
UEs	User Equipments
XQAM	Cross QAM

complex additive white Gaussian noise (AWGN), and the AWGN vectors are modeled as $\mathcal{CN}(0, \sigma^2 \mathbf{I}_{No})$, where $\sigma^2 = \mathrm{k_B T B_{No}}$, and $\mathrm{k_B}$, T, and $\mathrm{B_{No}}$, denote the Boltzmann constant, temperature in Kelvin, and receiver bandwidth, respectively.

A. PATHLOSS MODELING

In this subsection, the path loss modeling considered in analyzing the AG channels and vice-versa is presented. The path loss is expressed as [10]

$$\zeta_{\mathrm{AG_{dB}}} = \alpha_{\mathrm{AB}} 10 \log_{10} \mathrm{R_{AB}} + \eta_{\mathrm{AB}}, \tag{1}$$

where α_{AB}, $\mathrm{R_{AB}}$, and η_{AB} stand for the path loss exponent, distance and path loss at the reference point of the AG channel corresponding to the AB link with respect to (w.r.t.) $\mathrm{U_R}$, respectively. The absolute value of this path loss model is given by [15]

$$\begin{aligned}\zeta_{\mathrm{AG}} &= 10^{\frac{\zeta_{\mathrm{AG_{dB}}}}{10}} \\ &= 10^{\frac{Q}{10} + \frac{P}{10 + 10 p' \exp^{-q'(\theta_{\mathrm{ele}} - p')}}} \mathrm{R_{AB}^{\alpha_{AB}}} = \beta_{\mathrm{AB}} \mathrm{R_{AB}^{\alpha_{AB}}}, \end{aligned}\tag{2}$$

where $P = \eta_{\mathrm{LOS}} - \eta_{\mathrm{NLOS}}$, $Q = 10 \log 10 (\frac{4\pi f}{c})^2 + \eta_{\mathrm{NLOS}}$, and f and c denote the carrier frequency and speed of light, respectively. The elevation angle is given by $(\theta_{\mathrm{ele}}) = \frac{180}{\pi} \arctan(\frac{h_{\mathrm{UAV}}}{\mathrm{d_{AB}}})$, where h_{UAV} represents the altitude of UAV from the ground, $\mathrm{d_{AB}}$ denotes the distance between the nodes A and B, and $\mathrm{R_{AB}} = \sqrt{h_{\mathrm{UAV}}^2 + \mathrm{d_{AB}^2}}$. The values of η_{LOS}, η_{NLOS}, p', and q' depend on the propagation environment and are given in TABLE 3. There is a trade-off between the LOS propagation and path losses with the increase in h_{UAV} [15].

B. OUTDATED CSI MODEL

In practice, perfect CSI is not available at the transmitter. Due to the time-varying nature of the channel and also due to the mobility of the users, the Doppler frequency of the user is greater than the receiver processing time, resulting in the CSI being outdated [33]. Thus, the CSI received at the transmitter is considered to be delayed when fed back from the receiver due to non-zero feedback link delay. Consider $\hat{\mathbf{h}}_{\mathrm{AB}}^{\mathrm{k}}$ and $\mathbf{h}_{\mathrm{AB}}^{\mathrm{k}}$ represent the estimated and the actual channel vectors that are used for antenna selection and decoding, respectively. Since $\hat{\mathbf{h}}_{\mathrm{AB}}^{\mathrm{k}}$ is the outdated version of $\mathbf{h}_{\mathrm{AB}}^{\mathrm{k}}$, $\hat{\mathbf{h}}_{\mathrm{AB}}^{\mathrm{k}}$ when conditioned over $\mathbf{h}_{\mathrm{AB}}^{\mathrm{k}}$ follows a Gaussian distribution and is modeled as follows [33]:

$$\hat{\mathbf{h}}_{\mathrm{AB}}^{\mathrm{k}} = \rho_{\mathrm{AB}} \mathbf{h}^{\mathrm{k}}{}_{\mathrm{AB}} + \sqrt{1 - \rho_{\mathrm{AB}}^2}\, \mathbf{e}, \tag{3}$$

where $\rho_{\mathrm{AB}} \in (0, 1)$ represents the correlation coefficient between $\hat{\mathbf{h}}_{\mathrm{AB}}^{\mathrm{k}}$ and $\mathbf{h}_{\mathrm{AB}}^{\mathrm{k}}$, and the error is modeled as $\mathbf{e} \sim \mathcal{N}(0, I)$ [33], [34]. In the presence of Clarke's fading spectrum (band-limited), $\rho_{\mathrm{AB}} = \mathcal{J}_o(2\pi f_d T_d)$, where f_d is the Doppler frequency and T_d represents the delay spread of the feedback channels (i.e., the delay between relay selection and information retransmission instants). For Clarke's fading spectrum, $|\rho_{\mathrm{AB}}|$ does not decrease monotonically to zero as T_d increases but it fluctuates around zero as $T_d \to \infty$ [35]. Hence, in the analysis, we consider the impact of outdated CSI at all the nodes. Thus, via TAS, the antenna at the transmitter is selected as $||\hat{\boldsymbol{h}}_{\mathrm{B}\times 1}|| = \max_{1 \le j \le N_{\mathrm{A}}} \{||\hat{\boldsymbol{h}}_{\mathrm{B}\times \mathrm{j}}||\}$. In the analysis, it is considered that the S $\to$ $\mathrm{D_i}$ link is not available due to heavy shadowing.

The entire communication between S and $\mathrm{D_i}$ takes place in two-time slots. In the first slot, S broadcasts to $\mathrm{U_R}$ node. In the second time slot, $\mathrm{U_R}$ forwards the decoded and re-encoded information to the opportunistically scheduled UE $\mathrm{D_i}$. The signal received at $\mathrm{U_R}$ from the kth transmit antenna in the first time slot is expressed as

$$\mathbf{y}_{\mathrm{SU_R}} = \sqrt{P_{\mathrm{S}} \zeta_{\mathrm{SU_R}}} \mathbf{h}_{\mathrm{SU_R}}^{\mathrm{k}} x + \mathbf{n}_{\mathrm{SU_R}}, \tag{4}$$

where P_{S} is the transmit power, and path loss $\zeta_{\mathrm{SU_R}}$ is modeled as in (2). Notation $\mathbf{n}_{\mathrm{SU_R}}$ denotes the AWGN vector of S $\to$ $\mathrm{U_R}$ link. At $\mathrm{U_R}$, the received signal $\mathbf{y}_{\mathrm{SU_R}}$ is processed using the maximum ratio combiner. As the users are opportunistically scheduled, the received information at the ith UE ($\mathrm{D_i}$) after the transmit beam forming through the lth transmit antenna is expressed as

$$\mathbf{y}_{\mathrm{U_R D_i}} = \sqrt{P_R \zeta_{\mathrm{U_R D_i}}} \left(\mathbf{h}_{\mathrm{U_R D_i}}^{\mathrm{l}}\right)^H \mathbf{w}_{\mathrm{i}} x_{\mathrm{enc}} + \mathbf{n}_{\mathrm{U_R D_i}}, \tag{5}$$

where P_R is the transmitting power at the $\mathrm{U_R}$, path loss $\zeta_{\mathrm{U_R D_i}}$ is modeled as given in (2), x_{enc} denotes the re-encoded signal, and $\mathbf{n}_{\mathrm{U_R D_i}}$ stands for the AWGN vector of $\mathrm{U_R} \rightarrow \mathrm{D_i}$ link. The beam forming vector $\mathbf{w}_i = \frac{\mathbf{h}^{\mathrm{l}}_{\mathrm{U_R D_i}}}{||\mathbf{h}^{\mathrm{l}}_{\mathrm{U_R D_i}}||_F}$ is chosen according to the maximal ratio transmission principle. In practice, the time-varying channel changes dynamically, and thus it is expected to exhibit feedback delays in CSI between the transmitter and receiver. Delay is considered in antenna and user selection. Thus, the e2e SNR is given by

$$\hat{\gamma}^{(\mathrm{k,l})}_{e2e} = \hat{\gamma}^{(\mathrm{k,l})}_{\mathrm{SU_R D_i}} = \min\left\{\hat{\gamma}^{(\mathrm{k})}_{\mathrm{SU_R}}, \hat{\gamma}^{(\mathrm{l})}_{\mathrm{U_R D_i}}\right\}, \tag{6}$$

where $\hat{\gamma}^{(\mathrm{k})}_{\mathrm{SU_R}} = \frac{\gamma^{(\mathrm{k})}_{\mathrm{SU_R}}}{\chi_{\mathrm{SU_R}}}$, $\gamma^{(\mathrm{k})}_{\mathrm{SU_R}} = \overline{\gamma}_{\mathrm{SU_R}}||\mathbf{h}^{(\mathrm{k})}_{\mathrm{SU_R}}||^2$, $\chi_{\mathrm{SU_R}} = \frac{(2-\rho^2_{\mathrm{SU_R}})}{\rho^2_{\mathrm{SU_R}}}$, $\hat{\gamma}^{(\mathrm{l})}_{\mathrm{U_R D_i}} = \frac{\gamma^{(\mathrm{l})}_{\mathrm{U_R D_i}}}{\chi_{\mathrm{U_R D_i}}}$, $\gamma^{(\mathrm{l})}_{\mathrm{U_R D_i}} = \overline{\gamma}_{\mathrm{U_R D_i}}||\mathbf{w}^H_{\mathrm{i}}\mathbf{h}^{(\mathrm{l})}_{\mathrm{U_R D_i}}||^2$, and $\chi_{\mathrm{U_R D_i}} = \frac{(2-\rho^2_{\mathrm{U_R D_i}})}{\rho^2_{\mathrm{U_R D_i}}}$. Variables $\gamma^{(\mathrm{k})}_{\mathrm{SU_R}}$ and $\gamma^{(\mathrm{l})}_{\mathrm{U_R D_i}}$ denote the instantaneous SNRs, while $\overline{\gamma}^{(\mathrm{k})}_{\mathrm{SU_R}}$ and $\overline{\gamma}^{(\mathrm{l})}_{\mathrm{U_R D_i}}$ model the average SNRs corresponding to the $\mathrm{S} \rightarrow \mathrm{U_R}$ and $\mathrm{U_R} \rightarrow \mathrm{D_i}$ links, respectively. In (6), for a fixed $\hat{\gamma}^{(\mathrm{k})}_{\mathrm{SU_R}}$, $\hat{\gamma}^{(\mathrm{k})}$ is maximum when $\hat{\gamma}^{(\mathrm{l})}_{\mathrm{U_R D_i}}$ is maximized. Thus, antenna selection at $\mathrm{U_R}$ is independent of the antenna selection at S. Hence, the antenna index l at $\mathrm{U_R}$ is replaced with $\mathrm{l_{opt}}$.

III. OUTAGE PROBABILITY

OP is defined as the probability that the e2e SNR of the system falls below a predefined threshold where the transmission rate defines the threshold limit. The closed-form expression of OP is defined as

$$\begin{aligned} P_{out}(\gamma_{th}) &= P\Big(\max_{1\leq \mathrm{k} \leq N_S}\left\{\hat{\gamma}^{(\mathrm{k,l_{opt}})}_{e2e}\right\} < \gamma_{th}\Big) \\ &= P\Big(\max_{1\leq \mathrm{k} \leq N_S}\left\{\hat{\gamma}^{(\mathrm{k,l_{opt}})}_{\mathrm{SU_R D_i}}\right\} < \gamma_{th}\Big) \\ &= P\Big(\max_{1\leq \mathrm{k} \leq N_S}\Big(\min\left\{\hat{\gamma}^{(\mathrm{k})}_{\mathrm{SU_R}}, \hat{\gamma}^{(\mathrm{l_{opt}})}_{\mathrm{U_R D_i}}\right\}\Big) < \gamma_{th}\Big) \\ &= F_{\hat{\gamma}^{(\mathrm{k,l_{opt}})}_{e2e}}(\gamma_{th}) = F_{\hat{\gamma}^{(\mathrm{k,l_{opt}})}_{\mathrm{SU_R D_i}}}(\gamma_{th}), \end{aligned}$$

$$F_{\hat{\gamma}^{(\mathrm{k,l_{opt}})}_{\mathrm{SU_R D_i}}}(\gamma_{th}) = 1 - \Big(1 - F_{\hat{\gamma}^{(\mathrm{k})}_{\mathrm{SU_R}}}(\gamma_{th})\Big)\Big(1 - F_{\hat{\gamma}^{(\mathrm{l_{opt}})}_{\mathrm{U_R D_i}}}(\gamma_{th})\Big). \tag{7}$$

Proposition 1: The closed-form expression of the OP for a UAV-assisted multi-user system is given by

$$\begin{aligned} P^{(\gamma_{th})}_{out} &= 1 - \Big(1 - F_{\hat{\gamma}^{(\mathrm{k})}_{\mathrm{SU_R}}}(\gamma_{th})\Big)\Big(1 - F_{\hat{\gamma}^{(\mathrm{l_{opt}})}_{\mathrm{U_R D_i}}}(\gamma_{th})\Big), & (8) \\ &= 1 - C_1 C_2 \gamma^{t+s}_{th} e^{-\Delta_3 \gamma_{th}}, & (9) \end{aligned}$$

where C_1 and C_2 are given in TABLE 2, $\Delta_1 = \frac{m+1}{\lambda_{\mathrm{SU_R}}[1+m(1-\rho_{\mathrm{SU_R}})]}$, $\Delta_2 = \frac{p+1}{\lambda_{\mathrm{U_R D_i}}[1+p(1-\rho_{\mathrm{U_R D_i}})]}$, $\Delta_3 = \Delta_1 + \Delta_2$ and $\lambda_{AB} = \frac{\hat{\gamma}_{AB}}{m_{AB}}$.

Proof: Given in Appendix A. ■

A. ASYMPTOTIC ANALYSIS

At high SNR, system design parameters such as diversity order and coding gain are useful to model the system. Asymptotic OP expression is expressed at $\overline{\gamma} \rightarrow \infty$ as

$$P^{\infty}_{out}(\gamma_{th}) = \begin{cases} F_{\mathrm{SU_R}}\left(\frac{\gamma_{th}}{\overline{\gamma}}\right)^{d_1}, m_{\mathrm{SU_R}}N_S < m_{\mathrm{U_R D_i}}N_D \\ F_{\mathrm{U_R D_i}}\left(\frac{\gamma_{th}}{\overline{\gamma}}\right)^{d_2}, m_{\mathrm{SU_R}}N_S > m_{\mathrm{U_R D_i}}N_D \\ \left(F_{\mathrm{SU_R}} + F_{\mathrm{U_R D_i}}\right)\left(\frac{\gamma_{th}}{\overline{\gamma}}\right)^{d_3}, m_{\mathrm{SU_R}}N_S = m_{\mathrm{U_R D_i}}N_D \end{cases}$$

$$\begin{aligned} F_{\mathrm{SU_R}} = &\sum_{m=0}^{N_S-1}\sum_{n=0}^{m(M_{\mathrm{SU_R}}-1)}\binom{N_S-1}{m}\frac{\Gamma\left(M_{\mathrm{SU_R}}+n\right)}{M_{\mathrm{SU_R}}!\Gamma M_{\mathrm{SU_R}}} \\ &\times \frac{(-1)^a \Phi_{n,m,M_{\mathrm{SU_R}}}\left(1-\rho_{\mathrm{SU_R}}\right)^n}{\left[1+m(1-\rho_{\mathrm{SU_R}})\right]^{M_{\mathrm{SU_R}}+n}}\left(\frac{m_{\mathrm{SU_R}}}{k_{\mathrm{SU_R}}}\right)^{M_{\mathrm{SU_R}}}, \end{aligned} \tag{10}$$

$$\begin{aligned} F_{\mathrm{U_R D_i}} = &\sum_{p=0}^{N_R-1}\sum_{p=0}^{q(M_{\mathrm{U_R D_i}}-1)}\binom{N_R-1}{p}\frac{\Gamma\left(M_{\mathrm{U_R D_i}}+q\right)}{M_{\mathrm{U_R D_i}}!\Gamma M_{\mathrm{U_R D_i}}} \\ &\times \frac{(-1)^p \Phi_{q,p,M_{\mathrm{U_R D_i}}}\left(1-\rho_{\mathrm{U_R D_i}}\right)^q}{\left[1+p(1-\rho_{\mathrm{U_R D_i}})\right]^{M_{\mathrm{U_R D_i}}+q}}\left(\frac{m_{\mathrm{U_R D_i}}}{k_{\mathrm{U_R D_i}}}\right)^{M_{\mathrm{U_R D_i}}}, \end{aligned} \tag{11}$$

where $d_1 = m_{\mathrm{SU_R}}N_R$, $d_2 = m_{\mathrm{U_R D_i}}N_D$, and $d_3 = d_1 = d_2$ are the diversity orders of the system. Further, $k_{AB} = \frac{\overline{\gamma}_{AB}}{\overline{\gamma}}$.

IV. OPTIMIZATION OF SYSTEM PARAMETERS

A. OPTIMIZATION OF UAV LOCATION

In this section, we optimize the UAV location to attain MOP. At high SNR, the expression of OP of the $\mathrm{S} \rightarrow \mathrm{U_R} \rightarrow \mathrm{D_i}$ link is approximated as

$$P^{\infty}_{\gamma_{SRD}}(\gamma_{th}) = C_4\left(\frac{m_{\mathrm{SU_R}}}{k_{\mathrm{SU_R}}}\right)^{M_{\mathrm{SU_R}}N_S} + C_5\left(\frac{m_{\mathrm{U_R D_i}}}{k_{\mathrm{U_R D_i}}}\right)^{M_{\mathrm{U_R D_i}}N_R}, \tag{12}$$

where $C_4 = F_{\mathrm{SU_R}}(\frac{m_{\mathrm{SU_R}}}{k_{\mathrm{SU_R}}})^{-M_{\mathrm{SU_R}}}$, $C_5 = F_{\mathrm{U_R D_i}}(\frac{m_{\mathrm{U_R D_i}}}{k_{\mathrm{U_R D_i}}})^{-M_{\mathrm{U_R D_i}}}$. The $\mathrm{S} \rightarrow \mathrm{D_i}$ distance is maintained to be d_{tot}, $\mathrm{S} \rightarrow \mathrm{U_R}$ distance as $d_{\mathrm{SU_R}} = d_1$ and $\mathrm{U_R} \rightarrow \mathrm{D_i}$ distance as $d_{\mathrm{U_R D_i}} = (1 - d_{\mathrm{SU_R}}) = (d_{\mathrm{tot}} - d_1) = d_2$. After some manipulations, when $m_{\mathrm{SU_R}}N_S = m_{\mathrm{U_R D_i}}N_D = MN$, $P^{\infty}_{\gamma_{SRD}}(\gamma_{th})$ is expressed as

$$\begin{aligned} P^{\infty}_{\gamma_{SRD}}(\gamma_{th}) = &C_4\left(m_{\mathrm{SU_R}}\gamma_{\mathrm{th}}\right)^{M_{\mathrm{SU_R}}N_S}\left(\frac{1}{\overline{\gamma}_{\mathrm{SU_R}}}\right)^{M_{\mathrm{SU_R}}N_S} \\ &+ C_5\left(m_{\mathrm{U_R D_i}}\gamma_{\mathrm{th}}\right)^{M_{\mathrm{U_R D_i}}N_R}\left(\frac{1}{\overline{\gamma}_{\mathrm{U_R D_i}}}\right)^{M_{\mathrm{U_R D_i}}N_R}, \end{aligned} \tag{13}$$

$$\begin{aligned} P^{\infty}_{\gamma_{SRD}}(\gamma_{th}) = &C_4\left(\frac{m_{\mathrm{SU_R}}\gamma_{\mathrm{th}}\sigma^2_N}{P_S}\right)^{M_{\mathrm{SU_R}}N_S} \\ &\times \left(\beta_{\mathrm{SU_R}}(d_1)R_{\mathrm{SU_R}}(d_1)^{\alpha}\right)^{M_{\mathrm{SU_R}}N_S} \\ &+ C_5\left(\frac{m_{\mathrm{U_R D_i}}\gamma_{\mathrm{th}}\sigma^2_N}{P_R}\right)^{M_{\mathrm{U_R D_i}}N_R} \\ &\times \left(\beta_{\mathrm{U_R D_i}}(d_{\mathrm{tot}}-d_1)R_{\mathrm{U_R D_i}}(d_{\mathrm{tot}}-d_1)^{\alpha}\right)^{M_{\mathrm{U_R D_i}}N_R}, \end{aligned} \tag{14}$$

TABLE 2. Functional representations in arithmetic expressions.

Function	Representation
C_1	$\sum_{m=0}^{N_S-1}\sum_{n=0}^{m(M_{\mathrm{SU_R}}-1)}\sum_{j=0}^{n}\sum_{t=0}^{M_{\mathrm{SU_R}}+j-1}\binom{N_S-1}{m}\binom{n}{j}\frac{(-1)^{m+1}N_S\Gamma(M_{\mathrm{SU_R}}+n)\Phi_{n,m,M_{\mathrm{SU_R}}}}{t!\Gamma M_{\mathrm{SU_R}}(m+1)^{M_{\mathrm{SU_R}}+j-t}} \times \frac{\rho_{\mathrm{SU_R}}^t(1-\rho_{\mathrm{SU_R}})^{n-j}}{\lambda_{\mathrm{SU_R}}^j[1+m(1-\rho_{\mathrm{SU_R}})]^{n+t}},$
C_2	$\sum_{p=0}^{N_R-1}\sum_{q=0}^{m(M_{\mathrm{U_RD_i}}-1)}\sum_{r=0}^{q}\sum_{s=0}^{M_{\mathrm{U_RD_i}}+r-1}\binom{N_R-1}{p}\binom{q}{r}\frac{(-1)^{p+1}N_R\Gamma(M_{\mathrm{U_RD_i}}+q)\Phi_{q,p,M_{\mathrm{U_RD_i}}}}{s!\Gamma M_{\mathrm{U_RD_i}}(p+1)^{M_{\mathrm{U_RD_i}}+r-s}} \times \frac{\rho_{\mathrm{U_RD_i}}^s(1-\rho_{\mathrm{U_RD_i}})^{q-r}}{\lambda_{\mathrm{U_RD_i}}^r[1+p(1-\rho_{\mathrm{U_RD_i}})]^{q+s}},$
$C_3;\ \kappa;\ \kappa_1;\ \mathbb{P}(x);\ \mathbb{F}_1(a_1,b_1);$	$C_1C_2;\ t+s+\frac{1}{2};\ t+s+1;\ x+\Delta_3;\ {}_2F_1\Big(1,\kappa_1,\frac{3}{2},\frac{a_1}{b_1}\Big);$

TABLE 3. Simulation parameter values for the considered system [15], [42], [45].

Suburban areas parameters	
Parameter	Value
$\{\eta_{NLOS};\eta_{LOS}\}$	$\{21;0.1\}$ dB
α_{AB}	2
$\{p';q'\}$	$\{5.0188;0.3511\}$
h	120 m
d_{tot}	5 Km
f	5 GHz
c	3×10^8m/s
k	1.38×10^{-23}J/K
T	300K
$\mathrm{B_{No}}$	20MHz
ρ_{AB}	$[0,1]$
$\{P_L;L_p\}$	$\{80;68\}$ bit
R_b	4×10^5bps
$\{P_{ct};P_{cr}\}$	$\{10^{-4};5\times10^{-5}\}$W

where $R_{\mathrm{SU_R}}(d_1)=\sqrt{d_1^2+h^2}$, $PL_{\mathrm{SU_R}}=\beta_{\mathrm{SU_R}}(d_1)R_{\mathrm{SU_R}}(d_1)^{\alpha}$, $R_{\mathrm{SU_R}}(d_2)=\sqrt{d_2^2+h^2}$, and $PL_{\mathrm{SU_R}}=\beta_{\mathrm{U_RD_i}}(d_2)R_{\mathrm{U_RD_i}}(d_2)^{\alpha}$. Consider $d_1=d$. Equation (14) can be re-written as

$$P^{\infty}_{\gamma SRD_1}=C_6\Big(\beta_{\mathrm{SU_R}}(d)R_{\mathrm{SU_R}}(d)^{\alpha}\Big)^{M_{\mathrm{SU_R}}N_S}+C_7\Big(\beta_{\mathrm{U_RD_i}}(d_{\mathrm{tot}}-d)R_{\mathrm{U_RD_i}}(d_{\mathrm{tot}}-d)^{\alpha}\Big)^{M_{\mathrm{U_RD_i}}N_R}, \tag{15}$$

where $C_6=C_4(\frac{m_{\mathrm{SU_R}}\gamma_{\mathrm{th}}\sigma_N^2}{P_S})^{M_{\mathrm{SU_R}}N_S}$ and $C_7=C_5(\frac{m_{\mathrm{U_RD_i}}\gamma_{\mathrm{th}}\sigma_N^2}{P_R})^{M_{\mathrm{U_RD_i}}N_R}$.

CASE 1

In this case, OP is minimized w.r.t. UAV location. The objective function for the optimum relay location is formulated as

$$d^*=\arg\min_{d}\ P^{\infty}_{\gamma SRD_1}\quad \text{subject to}\quad 0<d_1<d_{\mathrm{tot}}. \tag{16}$$

CASE 2

In this case, OP is minimized w.r.t. to both the UAV relay location parameter d_1 and the UAV's height. The objective function for maximizing throughput is formulated as:

$$P^{\infty}_{\gamma SRD_2}=C_6\Big(\beta_{\mathrm{SU_R}}(d,h)R^{\alpha}_{\mathrm{SU_R}}\Big)^{M_{\mathrm{SU_R}}N_S}+C_7\Big(\beta_{\mathrm{U_RD_i}}(d_{\mathrm{tot}}-d,h)R^{\alpha}_{\mathrm{U_RD_i}}\Big)^{M_{\mathrm{U_RD_i}}N_R}, \tag{17}$$

$$d^*,h^*=\arg\min_{d,h}\ P^{\infty}_{\gamma SRD_2}$$

$$\text{subject to } 0<\{d\}<d_{\mathrm{tot}}, \tag{18}$$

$$0<\{h\}<h_{\max}. \tag{19}$$

where

$$\beta_{\mathrm{U_RD_i}}(d,h)=10^{\frac{Q}{10}+\frac{P}{10+10p'\exp^{-q'\left(\frac{180}{\pi}\arctan(\frac{h}{d})-p'\right)}}}, \tag{20}$$

$$\beta_{\mathrm{SU_R}}(d_{\mathrm{tot}}-d,h)=10^{\frac{Q}{10}+\frac{P}{10+10p'\exp^{-q'\left(\frac{180}{\pi}\arctan(\frac{h}{d_{\mathrm{tot}}-d})-p'\right)}}}, \tag{21}$$

$R^{\alpha}_{\mathrm{SU_R}}=(d^2+h^2)^{\frac{\alpha}{2}}$, and $R^{\alpha}_{\mathrm{U_RD_i}}=((d_{\mathrm{tot}}-d)^2+h^2)^{\frac{\alpha}{2}}$. The exact closed-form expression of the above objective function is mathematically intractable. Further, the objective function is non-linear, twice continuously differentiable, and involves a large number of variables. Hence, we employ a quasi-Newton method based LBFGS algorithm [36] to obtain the optimum values for d and h that minimize the OP. L-BFGS algorithm is very stable due to the line search procedure and converges faster than the stochastic gradient descent algorithm with automatic step size detection [37]. L-BFGS uses the approximated second-order gradient information to provide a faster convergence toward the minimum and thus shows effectiveness over other optimization algorithms [37]. In LBFGS algorithm, objective functions (15) and (17) with the constraints given (16), (18), and (19), respectively, are optimized. For the objective function $f(x)$, x_k and α_k are the input and step size at the kth step, respectively, and $x_{k+1}=x_k+\alpha_k p_k$, where α_k is chosen to satisfy Wolfe conditions [36], [38] and $p_k=-\mathbf{B}_k^{-1}\nabla f(x)=\mathbf{H}_k\nabla f(x)$ is the minimizer (step search direction for each k). $\mathbf{B}_k$ is the

Algorithm 1: LBFGS Algorithm for OP Minimization w.r.t. d and h

Input: $\vec{x} = [d, h]^T$; Lower bound $[b_1, b_2] = 0$, Upper bound $[u_1, u_2] = [d_{tot}, h_{\max}]$,
Output: $f(\vec{x}^*)$ (OptVal) and $\vec{x}^*$ (OptPosition)
Data: Initialization $q \leftarrow \nabla f(\vec{x})$ (gradient)
for $i = k-1, k-2, \ldots, k-m$ **do**
  $\alpha_i \leftarrow \rho_i s_i^T q$;
  $q \leftarrow q - \alpha_i y_i$;
end
$s_k = x_{k+1} - x_k = \alpha_k p_k$;
$y_k = \nabla f_{k+1} - \nabla f_k$;
$H_k^0 = \frac{s_{k-1}^T y_{k-1}}{y_{k-1}^T y_{k-1}} I$;
$z = H_k^0 q$
for $i = k-m, k-m+1, \ldots, k-1$ **do**
  $\beta_i \leftarrow \rho_i y_i^T z$;
  $z \leftarrow z + s_i(\alpha_i - \beta_i)$;
end
if $k > m$ **then**
  compute s_k and y_k until convergence
  terminate $z = H_k \nabla f(\vec{x})_k$
end

approximation for the Hessian matrix ($\mathbf{H}$). LBFGS is based on the BFGS recursion for the inverse Hessian as

$$\mathbf{H}_{k+1} = \left(I - \rho_k s_k y_k^T\right)\mathbf{H}_k\left(I - \rho_k y_k s_k^T\right) + \rho_k s_k s_k^T. \quad (22)$$

The pseudo algorithm for LBFGS is given in Algorithm 1.

V. ASER ANALYSIS

In this section, we obtain the ASER expressions for the higher-order QAM schemes using the CDF approach. For a digital modulation scheme, the CDF based generalized ASER is expressed as [39]

$$P_s(e) = -\int_0^\infty P_s'(e|\gamma) F_{\hat{\gamma}_{e2e}^{(\mathrm{k,l_{opt}})}}(\gamma) d\lambda, \quad (23)$$

where $P_s'(e|\gamma)$ is the first order derivative of the conditional symbol error probability (SEP) of a modulation scheme over the AWGN channel w.r.t.. instantaneous SNR (γ) and $F_{\gamma_{e2e}}(\gamma)$ is the CDF of the e2e SNR.

A. HEXAGONAL QAM SCHEME

The conditional SEP expression for M-ary HQAM scheme over AWGN channel takes the form [20]:

$$P_s^H(e|\gamma) = BQ\left(\sqrt{\alpha_h\gamma}\right) + \frac{2}{3}B_c Q^2\left(\sqrt{\frac{2\alpha_h\gamma}{3}}\right) - 2B_c Q\left(\sqrt{\alpha_h\gamma}\right) Q\left(\sqrt{\frac{\alpha_h\gamma}{3}}\right), \quad (24)$$

where the parameters B, B_c, and α_h of the considered HQAM are defined in [18] for different constellation points.

Proposition 2: The generalized ASER expression of HQAM for UAV assisted multi-user systems is expressed as

$$\begin{aligned}
P_s{}^H =& \frac{(B)}{2} - \frac{Bc}{3} - H_d\left(\frac{2\alpha_h}{3}\right)^{-1} {}_2F_1\left(1, 1, \frac{3}{2}, \frac{1}{2}\right) \\
&+ H_e \frac{2\alpha_h}{3}^{-1} + \left({}_2F_1\left(1, 1, \frac{3}{2}, \frac{3}{4}\right) + {}_2F_1\left(1, 1, \frac{3}{2}, \frac{1}{4}\right)\right) \\
&+ C_3\Bigg[(\kappa-1)! + \Bigg\{H_a\mathbb{P}\left(\frac{\alpha_h}{2}\right)^{-\kappa} - H_b\mathbb{P}\left(\frac{\alpha_h}{3}\right)^{-\kappa} \\
&\quad + H_c\mathbb{P}\left(\frac{\alpha_h}{6}\right)^{-\kappa}\Bigg\} + \Gamma(\kappa_1) \\
&\times \mathbb{P}\left(\frac{2\alpha_h}{3}\right)^{-\kappa_1}\Bigg\{H_d\mathbb{F}_1\left(\frac{\alpha_h}{3}, \mathbb{P}\left(\frac{2\alpha_h}{3}\right)\right) \\
&- H_e\left(\mathbb{F}_1\left(\frac{\alpha_h}{2}, \mathbb{P}\left(\frac{2\alpha_h}{3}\right)\right) + \mathbb{F}_1\left(\frac{\alpha_h}{6}, \mathbb{P}\left(\frac{2\alpha_h}{3}\right)\right)\right)\Bigg\}\Bigg]
\end{aligned} \quad (25)$$

where $H_a = \frac{(B_c - B)}{2}\sqrt{\frac{\alpha_h}{2\pi}}$, $H_b = \frac{B_c}{3}\sqrt{\frac{\alpha_h}{3\pi}}$, $H_c = \frac{B_c}{2}\sqrt{\frac{\alpha_h}{6\pi}}$, $H_d = \frac{2B_c\alpha_h}{9\pi}$, and $H_e = \frac{B_c\alpha_h}{2\sqrt{3}\pi}$, and $\Delta_8 = 2\sqrt{\Delta_6}$.

Proof: The proof is given in Appendix B. ■

B. RECTANGULAR QAM SCHEME

The conditional SEP of RQAM over AWGN channels takes the form [39, eq. (18)]

$$P_s{}^{RQAM}(e|\gamma) = 2\Big[R_1 Q\left(b_1\sqrt{\gamma}\right) + R_2 Q\left(b_2\sqrt{\gamma}\right) - 2R_1R_2 Q\left(b_1\sqrt{\gamma}\right)Q\left(b_2\sqrt{\gamma}\right)\Big], \quad (26)$$

where $R_1 = 1 - \frac{1}{M_I}$, $R_2 = 1 - \frac{1}{M_Q}$, $b_1 = \sqrt{\frac{6}{(M_I{}^2-1)+(M_Q^2-1)d_{IQ}{}^2}}$, and $b_2 = d_{IQ}b_1$. Further, M_I and M_Q indicate the in-phase and quadrature-phase constellation points, respectively. Additionally, $d_{IQ} = \frac{d_Q}{d_I}$, where d_I and d_Q are the in-phase and quadrature decision distances, respectively.

Proposition 3: The generalized ASER expression of RQAM for UAV assisted multi-user systems is expressed as

$$\begin{aligned}
P_s^R \approx& -R_1(R_2 - 1) - R_2(R_1 - 1) + \frac{R_1R_2b_1b_2r_3^{-1}}{\pi} \\
&\times \left\{{}_2F_1\left(1, 1, \frac{3}{2}, \frac{r_1}{r_3}\right) + {}_2F_1\left(1, 1, \frac{3}{2}, \frac{r_2}{r_3}\right)\right\} + C_3 \\
&\times \Bigg[\left(t + s - \frac{1}{2}\right)!\left\{-R_a\mathbb{P}(r_1)^{-\kappa} - R_b\mathbb{P}(r_2)^{-\kappa}\right\} + \Gamma(\kappa_1) \\
&\times \mathbb{P}(r_3)^{-\kappa_1} R_c\Big(\mathbb{F}_1(r_1, \mathbb{P}(r_3)) + \mathbb{F}_1(r_2, \mathbb{P}(r_3))\Big)\Bigg].
\end{aligned} \quad (27)$$

Here, $R_a = \frac{b_1R_1(R_2-1)}{\sqrt{2\pi}}$, $R_b = \frac{b_2R_2(R_1-1)}{\sqrt{2\pi}}$, $R_c = \frac{b_1b_2R_1R_2}{\sqrt{2\pi}}$, $r_1 = \frac{b_1{}^2}{2}$, $r_2 = \frac{b_2{}^2}{2}$, and $r_3 = \frac{b_1{}^2+b_2{}^2}{2}$. SQAM is a special case of RQAM and it is obtained by considering $M_I = M_Q = \sqrt{M}$ and $d_{IQ} = 1$.

Proof: Given in Appendix C. ■

C. CROSS QAM SCHEME

The conditional SEP for the 32-XQAM scheme is expressed as [40, eq. (21)]:

$$P_s{}^X(e|\gamma) = X_1 Q\left(\sqrt{2\kappa_x\gamma}\right) + \frac{4}{M_x} Q\left(2\sqrt{\kappa_x\gamma}\right) - X_2 Q^2\left(\sqrt{2\kappa_x\gamma}\right), \tag{28}$$

where $X_1 = 4 - \frac{6}{\sqrt{2M_x}}$, $X_2 = 4 - \frac{12}{\sqrt{2M_x}} + \frac{12}{M_x}$, $\kappa_x = \frac{48}{31M_x - 32}$, and $M_x = 32$. The generalized ASER for XQAM is obtained by taking the FOD of (28) and substituting the resultant expression along with (9) in (23). By using the identities [41, eq. (3.371), (7.522.9)], the generalized ASER for XQAM is expressed as

$$\begin{aligned} P_s^X \approx{}& X_3 + \frac{2}{M_x} + \frac{X_2}{2\pi}{}_2F_1\left(1, 1, \frac{3}{2}, \frac{1}{2}\right) \\ &+ C_3\Bigg[(\kappa-1)! \times \Bigg\{\sqrt{\frac{\kappa_x}{\pi}} X_3 \mathbb{P}(\kappa_x)^{-\xi} \\ &- \frac{4}{M_x}\sqrt{\frac{\kappa_x}{2\pi}}\mathbb{P}(2\kappa_x)^{-\xi}\Bigg\} \\ &- \frac{X_2\kappa_x\Gamma(\kappa_1)}{\pi}\mathbb{P}(2\kappa_x)^{-\xi}\mathbb{F}_1(\kappa_x, \mathbb{P}(2\kappa_x))\Bigg] \end{aligned} \tag{29}$$

where $X_3 = \frac{X_2 - X_1}{2}$ $u_{x_1} = \Delta + n + \frac{1}{2}$, $u_{x_2} = \Delta + n + j + 1$, $\beta_{x_1} = 2\psi_{\mathrm{SU_R}}\sqrt{\Delta_2}$, $\alpha_{x_1} = \psi_{\mathrm{SU_R}}\Delta_1 + \mathbb{P}(\kappa_x)$, and $\alpha_{x_2} = \psi_{\mathrm{SU_R}}\Delta_1 + \mathbb{P}(2\kappa_x)$.

ENERGY EFFICIENCY ANALYSIS

Energy efficiency (EE) quantifies the energy consumed in delivering data. EE is the ratio of total amount of data delivered to the total amount of energy consumed and is given by [42]

$$\eta = \frac{P_L p_s}{E_s} = \frac{P_L\left(1 - \bar{P}_s\right)}{E_s}, \tag{30}$$

where P_L is the length of the packet, p_s represents the probability of the successful received data at the receiver and E_s is the total energy consumption for transmitting the data, $\bar{P}_s$ is the symbol error rate of the considered modulation scheme, and

$$E_s = \frac{L_p P}{R_b}, \tag{31}$$

where L_p, P and R_b stand for the payload packet size, total power, and rate of transmission, respectively. For a MIMO cooperative relaying-based network, the total power is given by [43]:

$$P = P_s(1+\ell)\left[P_{\mathrm{ct}} + \sum_{n_1=1}^{N_t} P_{\mathrm{cr}}\right] + P_r(1+\ell) \times \left[\sum_{n_2=1}^{N_r} P_{\mathrm{ct}} + \sum_{n_3=1}^{N_d+1} P_{\mathrm{cr}}\right], \tag{32}$$

where N_t, N_r, N_d are the number of antennas at the source, relay, and destination nodes. Further, $\ell = (\frac{\zeta}{\xi} - 1)$ defines the loss factor of the power amplifier. Parameter ζ represents the drain efficiency of the amplifier [44] and ξ denotes the peak-to-average power ratio corresponding to the modulation associated with the respective constellation size [18]. Upon substituting the derived SER expressions of the considered modulation schemes, the EE of the respective modulation schemes is obtained.

VI. NUMERICAL AND SIMULATION RESULTS

In this section, the numerical results are illustrated by comparing the accuracy of the analytical expressions with the Monte-Carlo simulations. The optimum location and height of the UAV are validated through simulations. Unless otherwise stated, the following parameters are considered: antenna elements (AEs) as $\{N_{\mathrm{S}}, N_{\mathrm{R}}, N_{\mathrm{D_i}}\}$, where $N_{\mathrm{D_i}}$ denotes the number of ground users. Fading parameters (FPs) of the Nakagami-m channels are $\{m_{\mathrm{SU_R}}, m_{\mathrm{U_RD_i}}\}$, and the outdated CSI correlation coefficients are $\{\rho_{\mathrm{SU_R}}, \rho_{\mathrm{U_RD_i}}\}$. In the analysis, the system performance is investigated for the cases when the correlation between the actual and estimated CSI is near to perfect ($\rho_{AB} = 0.9999$), moderate $\rho_{AB} = 0.95$, and extremely low $\rho_{AB} = 0.9$. Abbreviations 'Ana.', 'Asym.', and 'Sim.' stand for the 'analytical results', 'asymptotic results,' and 'simulation results', respectively.

A. IMPACT OF OUTDATED CSI

The severity of the feedback errors over the OP w.r.t. transmit power (dBm) performance is shown in FIGURE 2 for two different AEs cases. Arbitrary correlation coefficients are considered for the OP results presented in FIGURE 2(a) for $\{N_{\mathrm{S}}, N_{\mathrm{R}}, N_{\mathrm{D_i}}\} = \{2, 1, 2\}$ with FPs $\{m_{\mathrm{SU_R}} = 1, m_{\mathrm{U_RD_i}} = 2\}$. Results illustrate that system performance degrades with the increase in outdated CSI. Under perfect CSI conditions $\{\rho_{\mathrm{SU_R}} = 1, \rho_{\mathrm{U_RD_i}} = 1\}$, for an OP of 10^{-3}, system has a power gain of $\approx$ 11 dBm and $\approx$ 14 dBm w.r.t. $\{\rho_{\mathrm{SU_R}} = 0.7, \rho_{\mathrm{U_RD_i}} = 0.2\}$ and $\{\rho_{\mathrm{SU_R}} = 0.1, \rho_{\mathrm{U_RD_i}} = 0.2\}$, respectively. The derived analytical results match tightly with the asymptotic results and are verified through simulation results. Results in FIGURE 2(b) illustrate the impact of symmetric and asymmetric CSI conditions over OP performance for $\{N_{\mathrm{S}}, N_{\mathrm{R}}, N_{\mathrm{D_i}}\} = \{2, 2, 2\}$ with FPs $\{m_{\mathrm{SU_R}} = 1, m_{\mathrm{U_RD_i}} = 1\}$. It is observed that S $\rightarrow$ $\mathrm{U_R}$ link CSI conditions affect the overall system performance. The system with $\{\rho_{\mathrm{SU_R}} = 0.5, \rho_{\mathrm{U_RD_i}} = 0.9\}$ presents similar performance to that one associated with $\{\rho_{\mathrm{SU_R}} = 0.5, \rho_{\mathrm{U_RD_i}} = 0.5\}$. The system with $\{\rho_{\mathrm{SU_R}} = 0.9, \rho_{\mathrm{U_RD_i}} = 0.9\}$ exhibits the performance gains of ≈ 1.5 dBm and ≈ 4.5 dBm for an OP of 10^{-5} w.r.t. to other cases associated with $\{\rho_{\mathrm{SU_R}} = 0.9, \rho_{\mathrm{U_RD_i}} = 0.5\}$, $\{\rho_{\mathrm{SU_R}} = 0.5, \rho_{\mathrm{U_RD_i}} = 0.9\}$, and $\{\rho_{\mathrm{SU_R}} = 0.5, \rho_{\mathrm{U_RD_i}} = 0.5\}$, respectively.

Impact of AEs over OP are investigated w.r.t. transmit power for $\{\rho_{\mathrm{SU_R}} = 0.9, \rho_{\mathrm{U_RD_i}} = 0.9\}$ in FIGURE 3. It is observed that with the increase in the $\mathrm{U_R}$ AEs and $\mathrm{D_i}$ users, OP decreases. Results are presented for $\{N_{\mathrm{S}}, N_{\mathrm{R}}, N_{\mathrm{D_i}}\} =$

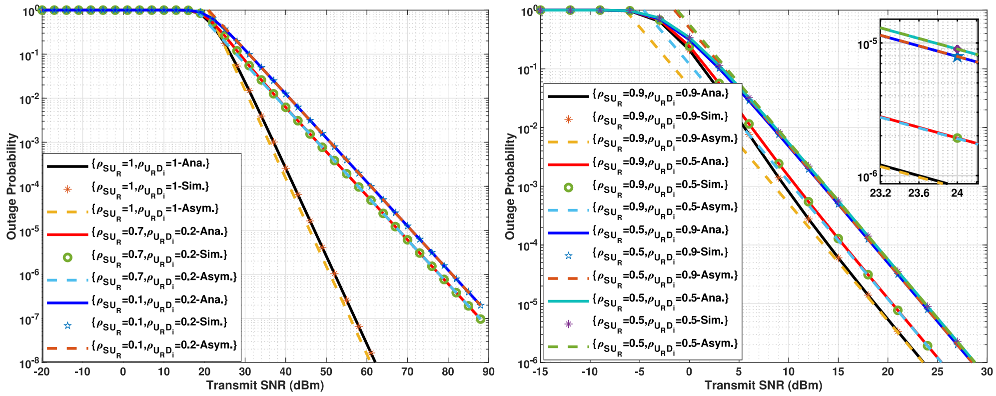

(a) $\{N_{\mathrm{S}}, N_{\mathrm{R}}, N_{\mathrm{D_i}}\} - \{2, 1, 2\}$.

(b) $\{N_{\mathrm{S}}, N_{\mathrm{R}}, N_{\mathrm{D_i}}\} - \{2, 2, 2\}$.

FIGURE 2. Outage probability vs transmit power (dBm) for different ρ_{AB} values.

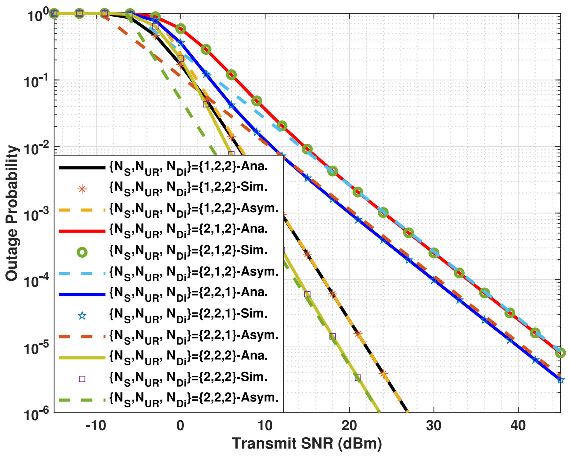

FIGURE 3. Outage probability vs transmit power (dBm) for various ACs with $\{\rho_{SU_R} = 0.9, \rho_{U_RD_i} = 0.9\}$ values.

$\{1, 2, 2\}$, $\{2, 1, 2\}$, $\{2, 2, 1\}$, $\{2, 2, 2\}$. For an OP of 10^{-3}, the system with $\{2, 2, 2\}$ AEs has a transmit power gain of ≈ 2 dBm, ≈ 10 dBm, and ≈ 14 dBm w.r.t. to $\{1, 2, 2\}$, $\{2, 1, 2\}$ and $\{2, 2, 1\}$. It is also observed that the reduction in $\mathrm{U_R}$ AEs degrades the system OP performance.

B. OPTIMIZATION OF UAV LOCATION

Optimization of $\mathrm{U_R}$ location to attain MOP under perfect and imperfect channel conditions is presented for a transmit SNR of 10 dBm in FIGURE 4. Under perfect CSI conditions, the optimization results are illustrated in FIGURE 4(a) for different antenna configurations. It is observed that the MOP of 3.58×10^{-12} for $\{N_{\mathrm{S}}, N_{\mathrm{R}}, N_{\mathrm{D_i}}\} = \{2, 2, 2\}$ system is attained when UAV is located exactly in middle between S and $\mathrm{U_R}$. For $\{N_{\mathrm{S}}, N_{\mathrm{R}}, N_{\mathrm{D_i}}\} = \{1, 2, 2\}$ system, MOP of 4.34×10^{-8} is attained when $\mathrm{U_R}$ is located closer to S whereas for $\{N_{\mathrm{S}}, N_{\mathrm{R}}, N_{\mathrm{D_i}}\} = \{2, 2, 1\}$ system, MOP of 5.2×10^{-2} is attained when $\mathrm{U_R}$ is located close to D_i. In FIGURE 4(b), impact of feedback errors is demonstrated for the $\{N_{\mathrm{S}}, N_{\mathrm{R}}, N_{\mathrm{D_i}}\} = \{2, 2, 2\}$ system. Results illustrate that the MOP is attained when $\mathrm{U_R}$ is located closer to the node whose link is severely affected by outdated CSI. For symmetric outdated CSI conditions, the system with $\{\rho_{\mathrm{SU_R}} = 0.9, \rho_{\mathrm{U_RD_i}} = 0.9\}$ attains MOP of 2.8×10^{-2} which is an increase in OP to 10^{-10} w.r.t. perfect CSI conditions which shows the severity of outdated CSI over system performance.

In FIGURE 5, the optimization of UAV altitude and location to attain MOP is illustrated for the $\{N_{\mathrm{S}}, N_{\mathrm{R}}, N_{\mathrm{D_i}}\} = \{1, 2, 2\}$ system with and without feedback errors at a transmit SNR of 5 dBm. In FIGURE 5(a), MOP results are plotted for perfect CSI conditions. It is observed that the optimum OP of 5.21×10^{-3} is obtained when $\mathrm{U_R}$ is located close to $\mathrm{D_i}$ at a distance of 4900 m and at a height of 118 m which increases LOS propagation, whereas in FIGURE 5(b), MOP results are plotted for $\{\rho_{\mathrm{SU_R}} = 0.2, \rho_{\mathrm{U_RD_i}} = 0.9\}$. Results illustrate that in the presence of severe outdated CSI impairment of the S $\rightarrow$ $\mathrm{U_R}$ link, the system attains the MOP of 7.68×10^{-2} at a distance of 2900 m and at height of 118 m. When there is a pronounced decline in channel correlation, the system reaches the MOP characteristic of the scenario where $\mathrm{U_R}$ is located closer proximity to S compared to the ideal situation.

For various QAM schemes in FIGURE 6, ASER analysis for even and odd constellations points are presented for the $\{N_{\mathrm{S}}, N_{\mathrm{R}}, N_{\mathrm{D_i}}\} = \{2, 2, 2\}$ system with $\{\rho_{\mathrm{SU_R}} = 0.9, \rho_{\mathrm{U_RD_i}} = 0.9\}$. The results plotted in FIGURE 6(a) illustrate the ASER analysis for even constellation points of HQAM and SQAM whereas in FIGURE 6(b), ASER analysis of odd bits of HQAM, RQAM, and XQAM are presented. For an ASER of 10^{-3}, 4-SQAM has a transmit power gain of ≈ 0.1 dBm w.r.t. 4-HQAM, whereas for 16 and 64 constellation points, HQAM has a transmit power gain of ≈ 0.45 dBm w.r.t. SQAM. For an ASER of 10^{-5}, 8-HQAM has a transmit power gain of ≈ 1 dBm w.r.t. 4×2-RQAM. For ASER of 10^{-4}, 32-HQAM has a transmit power gain of ≈ 0.7 dBm and ≈ 1.2 dBm w.r.t. 32-XQAM and 8×4-RQAM. This is due to the optimum 2D constellation of HQAM with low peak and average powers even for odd bits transmission.

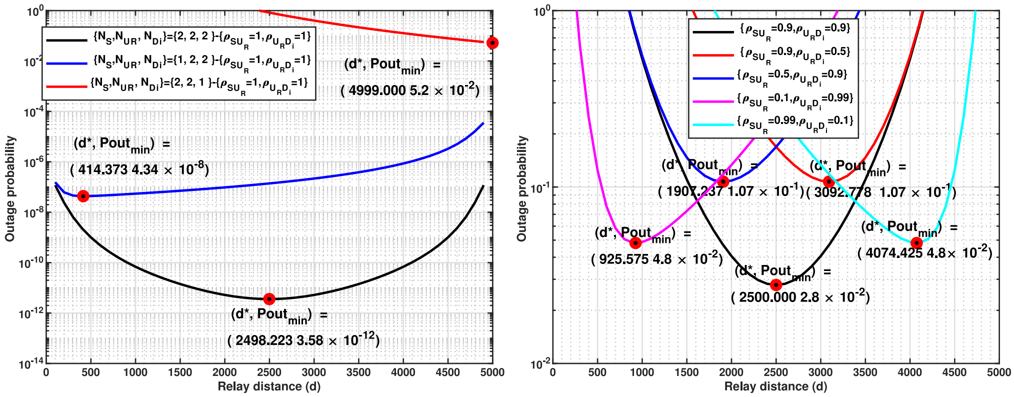

(a) Various antenna elements.

(b) $\{N_{\mathrm{S}}, N_{\mathrm{R}}, N_{\mathrm{D_i}}\} - \{2, 2, 2\}$-with Outdated CSI.

FIGURE 4. **Optimization of UAV location for minimum outage probability.**

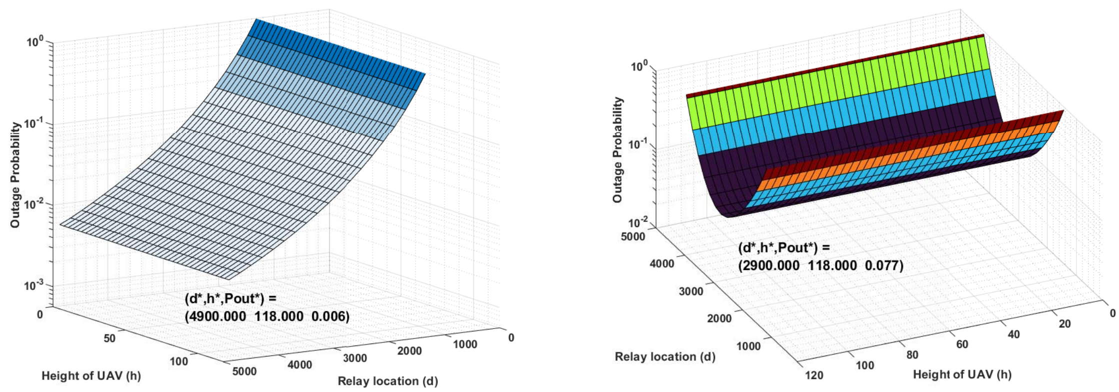

(a) $\{N_{\mathrm{S}}, N_{\mathrm{R}}, N_{\mathrm{D_i}}\} - \{1, 2, 2\}$-with Perfect CSI.

(b) $\{N_{\mathrm{S}}, N_{\mathrm{R}}, N_{\mathrm{D_i}}\} - \{1, 2, 2\}$-with Outdated CSI.

FIGURE 5. **Optimization of UAV location and height for minimum outage probability.**

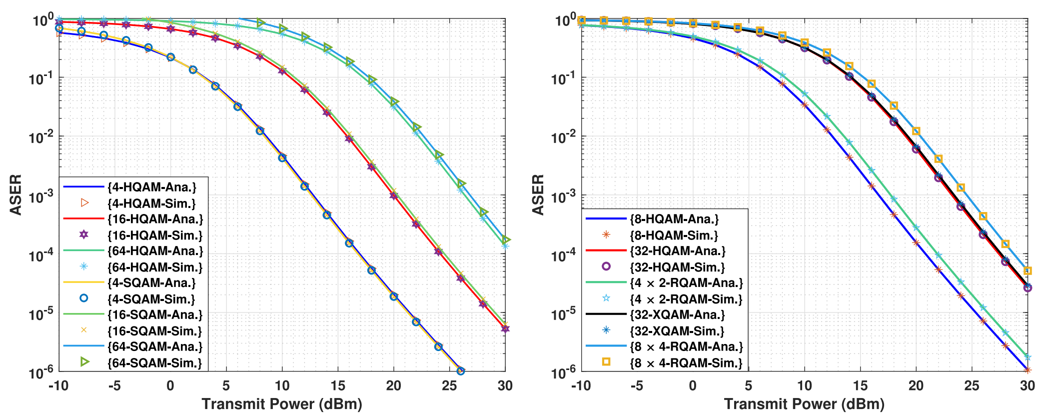

(a) Even constellation points.

(b) Odd constellation points.

FIGURE 6. **ASER analysis of even and odd bit constellation points.**

In FIGURE 7, the impact of feedback errors over ASER analysis of various QAM schemes is illustrated for various constellation points for the $\{N_{\mathrm{S}}, N_{\mathrm{R}}, N_{\mathrm{D_i}}\} = \{1, 4, 4\}$ system. Results illustrate an increase in the data rates with the error probability. In FIGURE 7(a) and FIGURE 7(b), results are presented with perfect and outdated CSI ($\{\rho_{\mathrm{SU_R}} = 0.2, \rho_{\mathrm{U_RD_i}} = 0.2\}$), respectively. The plotted results illustrate the performance degradation with the outdated CSI. 4-SQAM

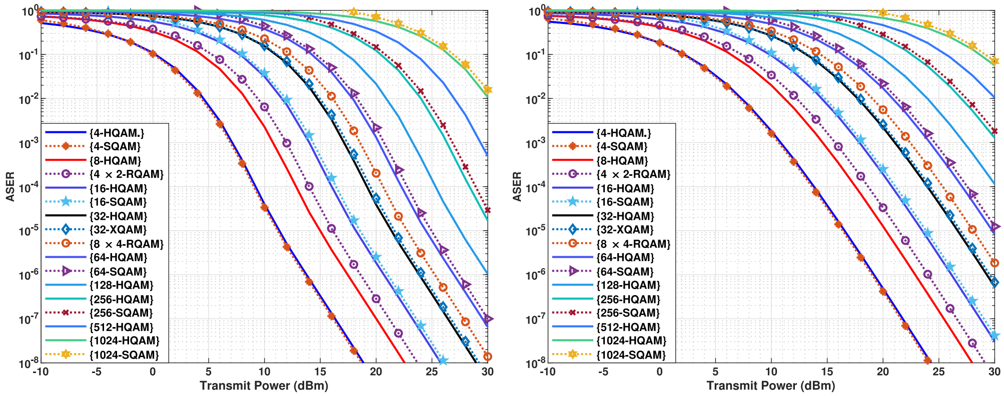

(a) Perfect CSI. (b) Outdated CSI.

FIGURE 7. ASER analysis of various constellation points with and without outdated CSI.

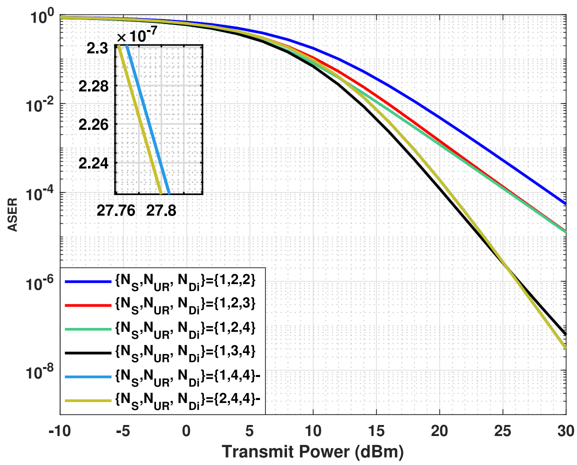

FIGURE 8. ASER analysis of 16 HQAM for $\{\rho_{SU_R} = 0.9, \rho_{U_RD_i} = 0.2\}$.

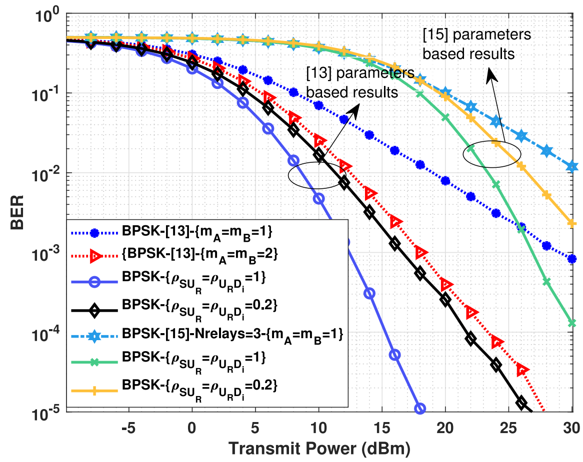

FIGURE 9. BER comparative results for BPSK.

provides a transmit power gain of ≈ 0.1 dBm over 4-HQAM. This is due to the presence of a large number of nearest neighborhoods for 4-HQAM as compared with the 4-SQAM. With the increase in constellation order from 8 to 1024, HQAM performs better w.r.t. other modulation schemes due to the optimum 2D hexagonal lattice with low peak and average energies for the same distance of separation between two constellation points.

In FIGURE 8, curves demonstrate the impact of $\mathrm{U_R}$ AEs and $\mathrm{D_i}$ users over ASER analysis of 16-HQAM scheme for $\{\rho_{\mathrm{SU_R}} = 0.9, \rho_{\mathrm{U_RD_i}} = 0.2\}$. Results are presented for the severely affected $\mathrm{U_R} \rightarrow \mathrm{D_i}$ link. It is observed that for an ASER of 10^{-4}, the increase of ground users from 2 to 4 is accompanied by a transmit power gain of 3 dBm. The curves demonstrate that the system performance improves with the increase in both $\mathrm{U_R}$ antennas and the ground users. For an ASER of 10^{-7}, $\{N_{\mathrm{S}}, N_{\mathrm{R}}, N_{\mathrm{D_i}}\} = \{2, 4, 4\}$ has a transmit power gain of ≈ 0.55 dBm over $\{N_{\mathrm{S}}, N_{\mathrm{R}}, N_{\mathrm{D_i}}\} = \{1, 3, 4\}$, whereas $\{N_{\mathrm{S}}, N_{\mathrm{R}}, N_{\mathrm{D_i}}\} = \{2, 4, 4\}$ exhibits similar performance to that of $\{N_{\mathrm{S}}, N_{\mathrm{R}}, N_{\mathrm{D_i}}\} = \{1, 4, 4\}$.

In FIGURE 9, BER of BPSK is presented as per the parameters presented in [13], [15] w.r.t. to presented work. For comparative analysis, $\{N_{\mathrm{S}}, N_{\mathrm{R}}, N_{\mathrm{D_i}}\} = \{2, 2, 2\}$ is considered. As in [13], the results for BPSK are shown for fading parameters $m = 1$ and $m = 2$. Even for highly uncorrelated channel links, our system performs better. Even though dual-hop multiple links for 3-UAV relay are considered, similar results are observed when the system is modeled as per [15]. The curves illustrate the degradation of the system performance with feedback errors. It is observed that for a BER of 10^{-2}, there is a degradation of system performance of about 2 and 2.5 dB with respect to [13] and [15], respectively.

ASER analysis of various HQAM constellation points is presented for the $\{N_{\mathrm{S}}, N_{\mathrm{R}}, N_{\mathrm{D_i}}\} = \{2, 2, 2\}$ system with $\{\rho_{\mathrm{SU_R}} = 0.9, \rho_{\mathrm{U_RD_i}} = 0.9\}$ in FIGURE 10. There is a trade-off between transmit power gain and the increase in constellation points. With the increase in constellation points from 4 to 64, the data rate increases, however, at the cost of increased error rate. The derived analytical results are corroborated by the Monte-Carlo simulations.

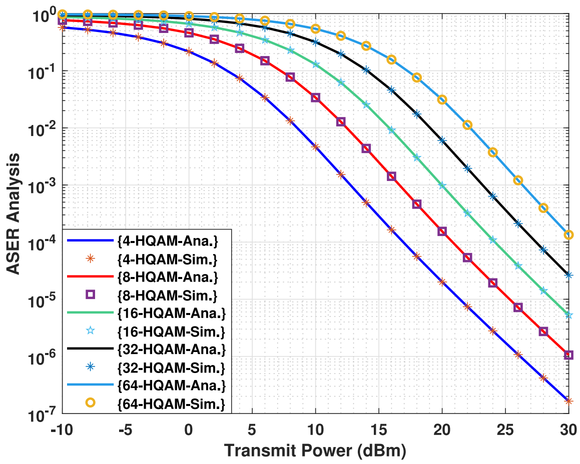

FIGURE 10. ASER Analysis of HQAM for various constellation points.

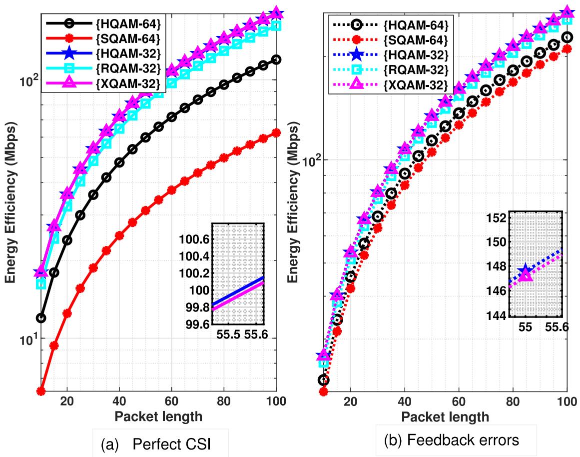

FIGURE 11. Energy efficiency of the system.

FIGURE 11 depicts the energy efficiency of the considered system model for HQAM, RQAM, and XQAM. All the results are reported at 30 dB transmit SNR. Results are obtained assuming the perfect channel state information scenario as well as under the influence of feedback errors ($\{\rho_{\mathrm{SU_R}} = 0.9, \rho_{\mathrm{U_R D_i}} = 0.2\}$). The value of ξ for various modulation schemes is provided in [18]. It is observed that HQAM attains better energy efficiency for even and odd constellation points over SQAM, RQAM, and XQAM. The curves illustrate that the overall energy efficiency of the system degrades with the outdated CSI. It is also observed that for odd constellation points, XQAM performs equivalently to HQAM. However, HQAM provides better efficiency due to low peak-to-average power.

VII. CONCLUSION

In this work, the performance of a dual-hop decode-and-forward UAV relaying system with multi-users is analyzed assuming MIMO antennas at the base station and UAV. The system is analyzed considering the detrimental effects of channel estimation errors over generalized Nakagami-m fading channels. The CDF of end-to-end SNR and closed-form expressions for OP, asymptotic OP, and ASER analysis of higher-order QAM schemes are derived and verified using Monte-Carlo simulations. Because of the optimal 2D hexagonal lattice, which exhibits low peak and average energies at identical separation distances between two constellation points, HQAM constellations outperform other modulation schemes. This superiority is confirmed through energy efficiency analysis. In addition, system performance is optimized by taking into account the dependence of MOP on the UAV location and height. Results illustrate the dominance of the S $\rightarrow$ $\mathrm{U_R}$ link CSI conditions over the entire system performance. Optimum performance in OP is dependent on the CEEs, antenna elements, and ground users. Analytical and simulation results clarify the impact of correlation parameters, multiple antennas, and fading parameters on the system performance.

APPENDIX A
PROOF OF PROPOSITION 1

Proof: Let $\hat{\gamma}^{(k)}_{\mathrm{SU_R}}$ represent the delayed version of $\hat{\gamma}^{(k)}_{\mathrm{SU_R}}$ by time τ, where τ is related to ρ through Clarke's fading model. The probability density function (PDF) of $\hat{\gamma}^{(\mathrm{k})}_{\mathrm{SU_R}}$ is expressed as

$$f_{\hat{\gamma}^{(\mathrm{k})}_{\mathrm{SU_R}}} = \int_0^\infty f_{\hat{\gamma}^{(\mathrm{k})}_{\mathrm{SU_R}}|\gamma^{(\mathrm{k})}_{\mathrm{SU_R}}}(y|x) f_{\gamma^{(\mathrm{k})}_{\mathrm{SU_R}}}(x)dx, \tag{33}$$

where

$$f_{\hat{\gamma}^{(\mathrm{k})}_{\mathrm{SU_R}}|\gamma^{(\mathrm{k})}_{\mathrm{SU_R}}}(y|x) = \frac{f_{\hat{\gamma}^{(\mathrm{k})}_{\mathrm{SU_R}}\gamma^{(\mathrm{k})}_{\mathrm{SU_R}}}(y, x)}{f_{\gamma^{(\mathrm{k})}_{\mathrm{SU_R}}}(x)}, \tag{34a}$$

$$f_{\gamma^{(\mathrm{k})}_{\mathrm{SU_R}}}(x) = N_R\left[F_{\gamma^{(\mathrm{k})}_{\mathrm{SU_R}}}(x)\right]^{N_S-1} f_{\gamma^{(\mathrm{k})}_{\mathrm{SU_R}}}(x). \tag{34b}$$

Also, $[F_{\gamma^{(\mathrm{k})}_{\mathrm{SU_R}}}(x)]^{N_S-1}$, is derived as in [39]. For a correlation coefficient ρ, the PDF of the actual SNR (γ_{AB}) conditioned over its estimate ($\hat{\gamma}_{AB}$) follows the non-central chi-square distribution with two degrees of freedom and is given by [34]

$$f_{\gamma_{AB},\hat{\gamma}_{AB}}(x, y) = \frac{\left(\frac{1}{\beta_{AB}}\right)^{M_{AB}+1}\left(\frac{xy}{\rho_{AB}}\right)^{\frac{M_{AB}-1}{2}}}{(1-\rho_{AB})\Gamma M_{AB}} \times \exp\left(-\frac{(x+y)}{(1-\rho_{AB})\beta_{AB}}\right) I_{M_{AB}-1}\left(\frac{2\sqrt{xy\rho_{AB}}}{(1-\rho_{AB})\beta_{AB}}\right), \tag{35}$$

where $M_{\mathrm{AB}} = m_{\mathrm{AB}}N_{\mathrm{B}}$, $\beta_{\mathrm{AB}} = \frac{\bar{\gamma}_{\mathrm{AB}}}{m_{\mathrm{AB}}}$. The PDF of $\hat{\gamma}^{(\mathrm{k})}_{\mathrm{SU_R}}$ is obtained by substituting (34), (35) in (33) and expressing the identity using [41, eq.(6.643.2)] as

$$f_{\hat{\gamma}^{(\mathrm{k})}_{\mathrm{SU_R}}}(x) = \sum_{m=0}^{N_S-1}\sum_{n=0}^{m(M_{\mathrm{SU_R}}-1)} \frac{(-1)^m N_S\binom{N_S-1}{m}\Gamma\left(M_{\mathrm{SU_R}}+n\right)}{\Gamma M_{\mathrm{SU_R}}\left(1-\rho_{\mathrm{SU_R}}\right)\beta_{\mathrm{SU_R}}^{\Delta_{m_1}}} \times \Phi_{n,m,M_{\mathrm{SU_R}}} e^{\frac{-x\beta_{\mathrm{SU_R}}^{-1}}{\left(1-\rho_{\mathrm{SU_R}}\right)}+\frac{\Delta_{m_2}}{2}} \frac{\Gamma\left(\mu_1+\vartheta_1+\frac{1}{2}\right)\mathrm{M}_{-\mu_1,\vartheta_1}\left(\Delta_{m_2}\right)}{\sqrt{a_1}\,\Gamma(2\vartheta_1+1)a_2^{\mu_1}}.$$

Notation $\Phi_{a,b,c}$ denotes the coefficient in the multinomial expansion $(\sum_{d=0}^{N-1}\frac{x^d}{d!})^r = \sum_{p=0}^{q(N-1)} \Phi_{p,q,r}\, x^a$ [39]. $\Delta_{m_1} = M_{\mathrm{SU_R}} + n + 1$, $\Delta_{m_2} = \frac{a_1}{a_2}$, $\mu_1 = \frac{M_{\mathrm{SU_R}}+2n}{2}$, $\vartheta_1 = \frac{M_{\mathrm{SU_R}}-1}{2}$, $a_1 = \frac{x\rho_1}{[(1-\rho_{\mathrm{SU_R}})\beta_{\mathrm{SU_R}}]^2}$, and $a_2 = \frac{1+m(1-\rho_{\mathrm{SU_R}})}{\beta_{\mathrm{SU_R}}(1-\rho_{\mathrm{SU_R}})}$. The above expression is further simplified by using the identities [41, eq.(9.220.2), eq.(9.210.1)] and [46] as

$$f_{\hat{\gamma}_{\mathrm{SU_R}}^{(\mathrm{k})}}(x) = \sum_{m=0}^{N_S-1}\sum_{n=0}^{m(M_{\mathrm{SU_R}}-1)}\sum_{j=0}^{n} \frac{(-1)^m N_S\binom{N_S-1}{m}\binom{n}{j}}{\Gamma M_{\mathrm{SU_R}}\gamma_{\mathrm{SU_R}}^{M_{\mathrm{SU_R}}+j}} \times \frac{\Gamma(M_{\mathrm{SU_R}}+n)}{\Gamma(M_{\mathrm{SU_R}}+j)}\frac{\Phi_{n,m,M_{\mathrm{SU_R}}}\rho_{\mathrm{SU_R}}^{j}(1-\rho_{\mathrm{SU_R}})^{n-j}}{[1+m(1-\rho_{\mathrm{SU_R}})]^{M_{\mathrm{SU_R}}+n+j}} \times x^{M_{\mathrm{SU_R}}+j-1}\mathrm{e}^{-\Delta_2\gamma_{th}}. \tag{36}$$

The PDF of $\gamma_{\mathrm{U_RD_i}}$ is obtained by following the above procedure and CDF is derived by evaluating $\int_0^x f(u)du$. The closed-form expression for OP as given in (9) is obtained by substituting the resultant expressions of $F_{\hat{\gamma}_{\mathrm{SU_R}}^{(\mathrm{k})}}(\gamma_{th})$ and $F_{\hat{\gamma}_{\mathrm{U_RD_i}}^{(\mathrm{l_{opt}})}}(\gamma_{th})$ in (7). ■

APPENDIX B
PROOF OF PROPOSITION 2

Proof: To derive the generalized closed-form ASER expression for HQAM, the CDF approach is followed. The first-order derivative (FOD) of $P_s^{HQAM}(e|\gamma)$ is obtained by taking the derivative of (24) w.r.t. γ and is expressed as

$$P_s{'}^{H}(e|\gamma) = H_a\gamma^{-\frac{1}{2}}e^{-\frac{\alpha_h\gamma}{2}} - H_b\gamma^{-\frac{1}{2}}e^{-\frac{\alpha_h\gamma}{3}} + H_c\gamma^{-\frac{1}{2}} \times e^{-\frac{\alpha_h\gamma}{6}} + H_d\alpha_h e^{-\frac{2\alpha_h\gamma}{3}}\,{}_1F_1\left(1,\frac{3}{2},\frac{\alpha_h}{3}\gamma\right) - H_e e^{\frac{-2\alpha_h\gamma}{3}} \times \left\{{}_1F_1\left(1,\frac{3}{2},\frac{\alpha_h}{2}\gamma\right) + {}_1F_1\left(1,\frac{3}{2},\frac{\alpha_h}{6}\gamma\right)\right\}. \tag{37}$$

Substituting (37) and (9) into (23) leads to:

$$\begin{aligned} P_s{}^{H} &= -\int_0^\infty P_s'(e|\gamma)F_{\gamma_{net}}(\gamma)d\gamma,\\ &= -\int_0^\infty P_s'(e|\gamma)\left(1 - C_3\gamma^{t+s}e^{-\Delta_3\gamma}\right)d\gamma,\\ &= -\int_0^\infty P_s'(e|\gamma)d\gamma - \int_0^\infty C_3P_s'(e|\gamma)\gamma^{t+s}e^{-\Delta_3\gamma}d\gamma \end{aligned} \tag{38}$$

In addition, I_1 and I_2 are expressed as

$$\begin{aligned} I_1 &= -\int_0^\infty \left(H_a\gamma^{-\frac{1}{2}}e^{-\frac{\alpha_h\gamma}{2}} - H_b\gamma^{-\frac{1}{2}}e^{-\frac{\alpha_h\gamma}{3}} + H_c\gamma^{-\frac{1}{2}} \times e^{-\frac{\alpha_h\gamma}{6}}\right)d\gamma\\ &\quad - \int_0^\infty \left(H_d e^{-\frac{2\alpha_h\gamma}{3}}\,{}_1F_1\left(1,\frac{3}{2},\frac{\alpha_h}{3}\gamma\right) - H_e \times e^{\frac{-2\alpha_h\gamma}{3}}\left\{{}_1F_1\left(1,\frac{3}{2},\frac{\alpha_h}{2}\gamma\right) + {}_1F_1\left(1,\frac{3}{2},\frac{\alpha_h}{6}\gamma\right)\right\}\right)d\gamma. I_2\\ &= C_3\left[\int_0^\infty \gamma^{t+s}e^{-\Delta_3\gamma}\left\{H_a\gamma^{-\frac{1}{2}}e^{-\frac{\alpha_h\gamma}{2}} - H_b\gamma^{-\frac{1}{2}}e^{-\frac{\alpha_h\gamma}{3}} + H_c\gamma^{-\frac{1}{2}}e^{-\frac{\alpha_h\gamma}{6}} + H_d\alpha_h e^{-\frac{2\alpha_h\gamma}{3}}\,{}_1F_1\left(1,\frac{3}{2},\frac{\alpha_h}{3}\gamma\right) - H_e \times e^{\frac{-2\alpha_h\gamma}{3}}\left\{{}_1F_1\left(1,\frac{3}{2},\frac{\alpha_h}{2}\gamma\right) + {}_1F_1\left(1,\frac{3}{2},\frac{\alpha_h}{6}\gamma\right)\right\}\right\}d\gamma\right]. \end{aligned} \tag{39}$$

The integrals in I_1 and I_2 are evaluated using the identities [41, eq. (3.351), (7.522.9)]:

$$I_1 = \frac{B}{2} - \frac{Bc}{3} - \frac{Bc}{3\pi}{}_2F_1\left(1,\frac{3}{2},\frac{1}{2}\gamma\right) + \frac{B_c}{3\sqrt(3)\pi} \times \left({}_2F_1\left(1,\frac{3}{2},\frac{3}{4}\gamma\right) + {}_2F_1\left(1,\frac{3}{2},\frac{1}{4}\gamma\right)\right). \tag{40}$$

$$I_2 = C_1\left[\left(t+s-\frac{1}{2}\right)!\left\{H_a\mathbb{P}\left(\frac{\alpha_h}{2}\right)^{-\kappa} - H_b\mathbb{P}\left(\frac{\alpha_h}{3}\right)^{-\kappa} + H_c\mathbb{P}\left(\frac{\alpha_h}{6}\right)^{-\kappa}\right\}\Gamma(\kappa_1)\mathbb{P}\left(\frac{2\alpha_h}{3}\right)^{-\kappa_1}\left\{H_d\mathbb{F}_1\left(\frac{\alpha_h}{3},\mathbb{P}\left(\frac{2\alpha_h}{3}\right)\right) - H_e\left(\mathbb{F}_1\left(\frac{\alpha_h}{2},\mathbb{P}\left(\frac{2\alpha_h}{3}\right)\right) + \mathbb{F}_1\left(\frac{\alpha_h}{6},\mathbb{P}\left(\frac{2\alpha_h}{3}\right)\right)\right)\right\}\right]. \tag{41}$$

Upon substituting (40) and (41) in (38), the generalized ASER expression for HQAM takes the value (25). ■

APPENDIX C
PROOF OF PROPOSITION 3

Proof: The FOD of (26) is obtained similarly to the FOD of HQAM conditional SEP as in (37). To derive the generalized ASER expression of RQAM, we substitute the FOD of (26) and (9) into (23) to obtain

$$\begin{aligned} P_s{}^{RQAM} &= -\int_0^\infty P_s'(e|\gamma)F_{\gamma_{net}}(\gamma)d\gamma,\\ &= -\int_0^\infty P_s'(e|\gamma)\left(1 - C_3\gamma^{t+s}e^{-\Delta_3\gamma}\right)d\gamma,\\ &= I_{R_1} + I_{R_2}. \end{aligned} \tag{42}$$

Further, I_{R_1} and I_{R_2} are expressed as:

$$I_{R_1} = -\int_0^\infty \left(R_a\gamma^{-\frac{1}{2}}e^{-r_1\gamma} + R_b\gamma^{-\frac{1}{2}}e^{-r_2\gamma} - R_c\left\{{}_1F_1\left(1,\frac{3}{2},r_1\gamma\right) + {}_1F_1\left(1,\frac{3}{2},r_2\gamma\right)\right\}\right)d\gamma, \tag{43}$$

$$I_{R_2} = -C_3\left[\int_0^\infty \gamma^{\left(t+s-\frac{1}{2}\right)}\left\{R_a e^{-\mathbb{P}(r1)\gamma} + R_b e^{-\mathbb{P}(r_2)\gamma}\right\}d\gamma - R_c\int_0^\infty \gamma^{(t+s)}e^{-\mathbb{P}(r_3)\gamma}\left\{{}_1F_1\left(1,\frac{3}{2},r_1\gamma\right) \times {}_1F_1\left(1,\frac{3}{2},r_2\gamma\right)\right\}d\gamma\right]. \tag{44}$$

The integrals in I_{R_1} and I_{R_2} are resolved by using the identities [41, eq. (3.371), (7.522.9)] and substituting them into (42) to get the closed-form expression (27). ■

ACKNOWLEDGMENT

The statements made herein are solely the responsibility of the authors.

REFERENCES

[1] Y. Zeng, Q. Wu, and R. Zhang, "Accessing from the sky: A tutorial on UAV communications for 5G and beyond," *Proc. IEEE*, vol. 107, no. 12, pp. 2327–2375, Dec. 2019.

[2] B. Li, Z. Fei, and Y. Zhang, "UAV communications for 5G and beyond: Recent advances and future trends," *IEEE Internet Things J.*, vol. 6, no. 2, pp. 2241–2263, Apr. 2018.

[3] C. Yan, L. Fu, J. Zhang, and J. Wang, "A comprehensive survey on UAV communication channel modeling," *IEEE Access*, vol. 7, pp. 107769–107792, 2019.

[4] "Technical specification group radio access network; study on enhanced LTE support for aerial vehicles (release 15), Version 15.0.0," 3GPP, Sophia, Antipolis, France, Rep. 36.777, Dec. 2017.

[5] M.-A. Russon, *Nokia and EE trial mobile base stations floating on drones to revolutionise rural 4G coverage*, Int. Bus. Times, New York, NY, USA, 2016.

[6] A. Fotouhi et al., "Survey on UAV cellular communications: Practical aspects, standardization advancements, regulation, and security challenges," *IEEE Commun.Surv. Tut.*, vol. 21, no. 4, pp. 3417–3442, Mar. 2019.

[7] M. Ding, P. Wang, D. López-Pérez, G. Mao, and Z. Lin, "Performance impact of LoS and NLoS transmissions in dense cellular networks," *IEEE Trans. Wireless Commun.*, vol. 15, no. 3, pp. 2365–2380, Mar. 2015.

[8] M. Hainzl, "Integrating UAVs into public safety LTE networks," *Tech. Rep.*, 2014.

[9] P. Zhan, K. Yu, and A. L. Swindlehurst, "Wireless relay communications with unmanned aerial vehicles: Performance and optimization," *IEEE Trans. Aerosp. Electron. Sys.*, vol. 47, no. 3, pp. 2068–2085, Jul. 2011.

[10] A. Al-Hourani, S. Kandeepan, and S. Lardner, "Optimal LAP altitude for maximum coverage," *IEEE Wireless Commun. Lett.*, vol. 3, no. 6, pp. 569–572, Dec. 2014.

[11] Y. Zeng, R. Zhang, and T. J. Lim, "Throughput maximization for UAV-enabled mobile relaying systems," *IEEE Trans. commun.*, vol. 64, no. 12, pp. 4983–4996, Dec. 2016.

[12] M. M. Azari, F. Rosas, K.-C. Chen, and S. Pollin, "Ultra reliable UAV communication using altitude and cooperation diversity," *IEEE Trans. Commun.*, vol. 66, no. 1, pp. 330–344, Jun. 2018.

[13] Y. Chen, W. Feng, and G. Zheng, "Optimum placement of UAV as relays," *IEEE Commun. Lett.*, vol. 22, no. 2, pp. 248–251, Feb. 2018.

[14] L. Sboui, H. Ghazzai, Z. Rezki, and M.-S. Alouini, "Achievable rates of UAV-relayed cooperative cognitive radio MIMO systems," *IEEE Access*, vol. 5, pp. 5190–5204, 2017.

[15] Y. Chen, N. Zhao, Z. Ding, and M.-S. Alouini, "Multiple UAVs as relays: Multi-hop single link versus multiple dual-hop links," *IEEE Trans. Wireless Commun.*, vol. 17, no. 9, pp. 6348–6359, Sep. 2018.

[16] S. Hanna, E. Krijestorac, H. Yan, and D. Cabric, "UAV swarms as amplify-and-forward MIMO relays," in *Proc. Int. Workshop Signal Process. Adv. Wireless Commun. (SPAWC)*, 2019, pp. 1–5.

[17] S. Hosseinalipour, A. Rahmati, and H. Dai, "Interference avoidance position planning in dual-hop and multi-hop UAV relay networks," *IEEE Trans. Wireless Commun.*, vol. 19, no. 11, pp. 7033–7048, Nov. 2020.

[18] P. K. Singya, P. Shaik, N. Kumar, V. Bhatia, and M.-S. Alouini, "A survey on higher-order QAM constellations: Technical challenges, recent advances, and future trends," *IEEE Open J. Commun. Soc.*, vol. 2, pp. 617–655, 2021.

[19] S. Parvez, P. K. Singya, and V. Bhatia, "On impact of imperfect CSI over hexagonal QAM for TAS/MRC-MIMO cooperative relay network," *IEEE Commun. Lett.*, vol. 23, no. 10, pp. 1721–1724, Oct. 2019.

[20] S. Parvez, P. K. Singya, and V. Bhatia, "On ASER analysis of energy efficient modulation schemes for a device-to-device MIMO relay network," *IEEE Access*, vol. 8, pp. 2499–2512, 2020.

[21] K. K. Garg, P. Singya, and V. Bhatia, "Performance analysis of NLOS ultraviolet communications with correlated branches over turbulent channels," *J. Opt. Commun. Netw.*, vol. 11, no. 11, pp. 525–535, Nov. 2019.

[22] P. Shaik, K. K. Garg, and V. Bhatia, "On impact of imperfect channel state information on dual-hop nonline-of-sight ultraviolet communication over turbulent channel," *Opt. Eng.*, vol. 59, no. 1, pp. 1–14, Jan. 2020.

[23] K. K. Garg, P. Shaik, and V. Bhatia, "Performance analysis of cooperative relaying technique for non-line-of-sight UV communication system in the presence of turbulence," *Opt. Eng.*, vol. 59, no. 5, May 2020, Art. no. 055101.

[24] P. K. Singya, N. Kumar, V. Bhatia, and M.-S. Alouini, "On the performance analysis of higher order QAM schemes over mixed RF/FSO systems," *IEEE Trans. Veh. Technol.*, vol. 69, no. 7, pp. 7366–7378, Jul. 2020.

[25] K. K. Garg, P. Shaik, V. Bhatia, and O. Krejcar, "On the performance of a relay assisted hybrid RF-NLOS UVC system with imperfect channel estimation," *J. Opt. Commun. Netw.*, vol. 14, no. 4, pp. 177–189, Apr. 2022.

[26] P. K. Singya and M.-S. Alouini, "Performance of UAV-assisted multiuser terrestrial-satellite communication system over mixed FSO/RF channels," *IEEE Trans. Aerosp. Electron. Sys.*, vol. 58, no. 2, pp. 781–796, Apr. 2021.

[27] A. Kumar, S. Majhi, and H.-C. Wu, "Physical-layer security of underlay MIMO-D2D communications by null steering method over Nakagami-*m* and norton fading channels," *IEEE Trans. Wireless Commun.*, vol. 21, no. 11, pp. 9700–9711, Nov. 2022.

[28] J. N. Laneman, D. N. Tse, and G. W. Wornell, "Cooperative diversity in wireless networks: Efficient protocols and outage behavior," *IEEE Trans. Inf. theory*, vol. 50, no. 12, pp. 3062–3080, Dec. 2004.

[29] M. K. Simon and M.-S. Alouini, *Digital Communication over Fading Channels*, vol. 95. Hoboken, NJ, USA: Wiley, Inc., 2005,

[30] W. Khawaja, I. Guvenc, and D. Matolak, "UWB channel sounding and modeling for UAV air-to-ground propagation channels," in *Proc. IEEE Global Commun. Conf. (GLOBECOM)*, 2016, pp. 1–7.

[31] E. Yanmaz, R. Kuschnig, and C. Bettstetter, "Achieving air-ground communications in 802.11 networks with three-dimensional aerial mobility," in *Proc. IEEE INFOCOM*, Apr. 2013, pp. 120–124.

[32] M. Nakagami, "The *m*-distribution—A general formula of intensity distribution of rapid fading," in *Proc. Statist. Method. Radio Wave Propagat.*, 1960, pp. 3–36.

[33] P. Shaik, P. K. Singya, K. K. Garg, and V. Bhatia, "Outage probability analysis of SWIPT device-to-device MIMO relay systems with outdated CSI," in *Proc. IEEE Wireless Commun. Netw. Conf. (WCNC)*, 2021, pp. 1–6.

[34] N. Yang, M. Elkashlan, P. L. Yeoh, and J. Yuan, "Multiuser MIMO relay networks in Nakagami-m fading channels," *IEEE Trans. Commun.*, vol. 60, no. 11, pp. 3298–3310, Nov. 2012.

[35] Y. Ma, D. Zhang, A. Leith, and Z. Wang, "Error performance of transmit beamforming with delayed and limited feedback," *IEEE Trans. Wireless Commun.*, vol. 8, no. 3, pp. 1164–1170, Mar. 2009.

[36] J. Nocedal and S. J. Wright, *Numerical Optimization*. New York, NY, USA: Springer, Aug. 1999.

[37] Q. V. Le, J. Ngiam, A. Coates, A. Lahiri, B. Prochnow, and A. Y. Ng, "On optimization methods for deep learning," in *Proc. Int. Conf. Mach. Learn.*, 2011, pp. 265–272.

[38] M. J. Kochenderfer and T. A. Wheeler, *Algorithms for Optimization*. Cambridge, MA, USA: MIT Press, Mar. 2019.

[39] P. Shaik, P. K. Singya, and V. Bhatia, "Performance analysis of QAM schemes for non-regenerative cooperative MIMO network with transmit antenna selection," *AEU-Int. J. Electron. Commun.*, vol. 107, pp. 298–306, Jul. 2019.

[40] X.-C. Zhang, H. Yu, and G. Wei, "Exact symbol error probability of cross-QAM in AWGN and fading channels," *EURASIP J. Wireless Commun. Netw.*, vol. 2010, pp. 917–954, Nov. 2010.

[41] I. S. Gradshteyn and I. M. Ryzhik, *Table of Integrals, Series, and Products*. Waltham MA, USA: Academic Press, 2014.

[42] M. Al-Kali, L. Yu, D. Samb, C. Liu, and D. Wang, "Performance analysis for energy efficiency in wireless cooperative relay networks," in *Proc. Int. Conf. Commun. Technol*, 2012, pp. 423–427.

[43] S. Cui, A. J. Goldsmith, and A. Bahai, "Energy-efficiency of MIMO and cooperative MIMO techniques in sensor networks," *IEEE J. Sel. Areas Commun.*, vol. 22, no. 6, pp. 1089–1098, Aug. 2004.

[44] T. H. Lee, *The Design of CMOS Radio-Frequency Integrated Circuits*. Cambridge, U.K.: Cambridge Univ. Press, Dec. 2003.

[45] Crossbow Corporation. "Mica2 datasheet [eb/ol]." 2008. [Online]. Available: http://www.eol.ucar.edu/rtf/facilities/isa/internal/CrossBow/DataSheets/mica2.pdf

[46] I. Wolfram Research. "Wolfram research-functions." 2010. [Online]. Available: http://functions.wolfram.com/07.20.03.0025.01

PARVEZ SHAIK (Member, IEEE) received the Ph.D. degree in electrical engineering from the Indian Institute of Technology (IIT) Indore, India. Following his doctorate, he served as a Research Associate with IIT Indore and a Visiting Postdoctoral Fellow with IISc Bangalore. He is currently a Postdoctoral Research Associate with Texas A&M University at Qatar. His research focuses on various aspects of communication networks, such as MIMO cooperative networks, terrestrial and non-terrestrial communications, RF and optical communications (including NOn-LOS UVC and VLC), IRS, and deep learning. He acted as the Co-Chair for IEEE ANTS 2022. He is a Peer Reviewer for several top-tier journals, including IEEE TRANSACTIONS ON VEHICULAR TECHNOLOGY, IEEE TRANSACTIONS ON COMMUNICATIONS, IEEE COMMUNICATIONS LETTERS, and *System*.

CIHAT KEÇECI received the B.S. (Hons.) and M.S. degrees in electrical and electronics engineering from Bogazici University, Istanbul, Turkey, in 2017 and 2020, respectively. He is currently pursuing the Ph.D. degree in electrical and computer engineering with Texas A&M University, College Station, TX, USA. He was with the Scientific and Technological Research Council of Turkey, Informatics and Information Security Research Center, Izmit, Kocaeli, Turkey. His research interests include machine learning, smart grids, and wireless communications.

KAMAL K. GARG received the M.Tech. degree in signal processing from the Netaji Subhash Institute of Technology, New Delhi, India, in 2002, and the Ph.D. degree from the Indian Institute of Technology Indore, India, in 2022. He currently serves as a Faculty Member with Pandit Deendayal Energy University, Gandhinagar, India. With over 15 years of experience in the field of satellite mobile communications, he has contributed significantly to this industry. He also held the position of Faculty Member with the Jaypee Institute of Technology, Noida, India, from 2002 to 2007. His research interests encompass signal processing, as well as the design and performance analysis of RF and optical wireless communication systems. He is an Esteemed Reviewer for prominent academic journals and conferences, including IEEE, OSA, and *Optica*.

MUHAMMAD ISMAIL (Senior Member, IEEE) received the B.Sc. (Hons.) and M.Sc. degrees in electrical engineering (electronics and communications) from Ain Shams University, Cairo, Egypt, in 2007 and 2009, respectively, and the Ph.D. degree in electrical and computer engineering from the University of Waterloo, Waterloo, ON, Canada, in 2013. He is currently an Assistant Professor with the Department of Computer Science, Tennessee Tech University, Cookeville, TN, USA. He was a co-recipient of the Best Paper Awards in the IEEE ICC 2014, the IEEE Globecom 2014, the SGRE 2015, the Green 2016, IEEE IS 2020, and the Best Conference Paper Award from the IEEE Communications Society Technical Committee on Green Communications and Networking at the IEEE ICC 2019. He was the Workshop Co-Chair of the IEEE Greencom 2018, the TPC Co-Chair of the IEEE VTC 2017 and 2016, the Publicity and Publication Co-Chair of the CROWNCOM 2015, and the Web-Chair of the IEEE INFOCOM 2014. He is an Associate Editor for the IEEE INTERNET OF THINGS JOURNAL and the IEEE TRANSACTIONS ON GREEN COMMUNICATIONS AND NETWORKING. He was an Associate Editor for the *IET Communications* and *Physical Communication*. He was an Editorial Assistant of the IEEE TRANSACTIONS ON VEHICULAR TECHNOLOGY from 2011 to 2013. He has been a technical reviewer of several IEEE conferences and journals.

ERCHIN SERPEDIN (Fellow, IEEE) is a Full Professor with the Electrical and Computer Engineering Department, Texas A&M University at College Station, College Station, TX, USA. His current research interests include signal processing, machine learning, artificial intelligence, cyber security, smart grids, and wireless communications. He served as an Associate Editor for more than 12 journals, including journals, such as the IEEE TRANSACTIONS ON INFORMATION THEORY, IEEE TRANSACTIONS ON SIGNAL PROCESSING, IEEE TRANSACTIONS ON COMMUNICATIONS, IEEE SIGNAL PROCESSING LETTERS, IEEE COMMUNICATIONS LETTERS, IEEE TRANSACTIONS ON WIRELESS COMMUNICATIONS, *IEEE Signal Processing Magazine*, *Signal Processing* (Elsevier), *Physical Communication* (Elsevier), and *EURASIP Journal on Advances in Signal Processing*.